Article

SOURCE DATA | TRANSPARENT PROCESS | OPEN ACCESS

EMBO reports

Loss of TMEM106B potentiates lysosomal and FTLD-like pathology in progranulin-deficient mice

Georg Werner[1], Markus Damme[2], Martin Schludi[3], Johannes Gnörich[4], Karin Wind[4], Katrin Fellerer[1], Benedikt Wefers[3,5], Wolfgang Wurst[3,5,6], Dieter Edbauer[3], Matthias Brendel[4], Christian Haass[1,3,6,*] & Anja Capell[1,**]

Abstract

Single nucleotide polymorphisms (SNPs) in *TMEM106B* encoding the lysosomal type II transmembrane protein 106B increase the risk for frontotemporal lobar degeneration (FTLD) of *GRN* (progranulin gene) mutation carriers. Currently, it is unclear if progranulin (PGRN) and TMEM106B are synergistically linked and if a gain or a loss of function of TMEM106B is responsible for the increased disease risk of patients with *GRN* haploinsufficiency. We therefore compare behavioral abnormalities, gene expression patterns, lysosomal activity, and TDP-43 pathology in single and double knockout animals. $Grn^{-/-}$/$Tmem106b^{-/-}$ mice show a strongly reduced life span and massive motor deficits. Gene expression analysis reveals an upregulation of molecular signature characteristic for disease-associated microglia and autophagy. Dysregulation of maturation of lysosomal proteins as well as an accumulation of ubiquitinated proteins and widespread p62 deposition suggest that proteostasis is impaired. Moreover, while single $Grn^{-/-}$ knockouts only occasionally show TDP-43 pathology, the double knockout mice exhibit deposition of phosphorylated TDP-43. Thus, a loss of function of TMEM106B may enhance the risk for *GRN*-associated FTLD by reduced protein turnover in the lysosomal/autophagic system.

Keywords FTD; neurodegeneration; progranulin; TDP-43; TMEM106B
Subject Categories Molecular Biology of Disease; Neuroscience
DOI 10.15252/embr.202050241 | Received 17 February 2020 | Revised 5 August 2020 | Accepted 10 August 2020 | Published online 14 September 2020
EMBO Reports (2020) 21: e50241

See also: **X Zhou *et al***, **T Feng *et al*** and **EL Clayton & AM Isaacs** (October 2020)

Introduction

Frontotemporal lobar degeneration (FTLD) is the second most common pre-senile neurodegenerative disease after Alzheimer's disease and is predominantly characterized by either tau or TAR DNA-binding protein 43 (TDP-43) depositions. Clinically, FTLD-TDP patients present with behavior and personality changes as well as speech disabilities (Snowden *et al*, 2006). In addition, many patients show an overlap with motor neuron diseases like amyotrophic lateral sclerosis (ALS) (Hardy & Rogaeva, 2014). A strong family history of dementia is present in FTD patients, implicating a significant genetic component. *C9orf72* repeat expansions (DeJesus-Hernandez *et al*, 2011; Renton *et al*, 2011) and progranulin (PGRN) haploinsufficiency are common causes of familial FTLD with TDP-43 pathology (FTLD-TDP) (Baker *et al*, 2006; Cruts *et al*, 2006; Gass *et al*, 2006). PGRN appears to exhibit neurotrophic and anti-inflammatory activities (Bateman *et al*, 2018). In addition, loss of PGRN is linked to dysfunctional lysosomal degradation and autophagy (Chang *et al*, 2017; Kao *et al*, 2017). While patients with PGRN haploinsufficiency show lysosomal abnormalities and present with some biochemical phenotypes of neuronal ceroid lipofuscinosis (NCL) (Gotzl *et al*, 2014; Ward *et al*, 2017), homozygous mutations leading to total loss of PGRN result in classical NCL (Smith *et al*, 2012; Almeida *et al*, 2016). PGRN is upregulated upon lysosomal dysfunction (Capell *et al*, 2011) and co-regulated with other lysosomal genes (Sardiello *et al*, 2009; Belcastro *et al*, 2011). Furthermore, PGRN is transported to lysosomes (Hu *et al*, 2010; Zhou *et al*, 2015) where it is processed by lysosomal proteases to granulin peptides (Holler *et al*, 2017; Lee *et al*, 2017; Zhou *et al*, 2017b). Lysosomal gene expression in *Grn* knockout mice is upregulated during aging (Gotzl *et al*, 2014; Klein *et al*, 2017) or injury (Tanaka *et al*, 2013, 2017; Beel *et al*, 2017). In line with lysosomal dysfunction in *GRN*-associated FTLD, aged *Grn* knockout mice are characterized by accumulation of lipofuscin, saposin D, the autophagy markers SQSTM1/p62 and ubiquitin. It is still puzzling that TDP-43

1 Metabolic Biochemistry, Biomedical Center (BMC), Faculty of Medicine, Ludwig-Maximilians-Universität München, Munich, Germany
2 Institute of Biochemistry, Kiel University, Kiel, Germany
3 German Center for Neurodegenerative Diseases (DZNE), Munich, Germany
4 Department of Nuclear Medicine, University Hospital, Ludwig-Maximilians-Universität München, Munich, Germany
5 Institute of Developmental Genetics, Helmholtz Zentrum München, German Research Center for Environmental Health, Neuherberg, Germany
6 Munich Cluster for Systems Neurology (SyNergy), Munich, Germany
*Corresponding author. Tel: +49 89440046550; E-mail: christian.haass@mail03.med.uni-muenchen.de
**Corresponding author. Tel: +49 89440046534; E-mail: anja.capell@mail03.med.uni-muenchen.de

pathology is abundant in *GRN* patients, but only occasionally observed in aged *Grn* knockout mice (Ahmed *et al*, 2010; Yin *et al*, 2010a; Ghoshal *et al*, 2012; Petkau *et al*, 2012; Wils *et al*, 2012; Gotzl *et al*, 2014; Tanaka *et al*, 2014).

The high variability in age of onset as well as the incomplete penetrance of *GRN* mutations led to the search for genetic risk factors in a genome-wide association study (GWAS), which identified single nucleotide polymorphisms (SNPs) in the *TMEM106B* locus that segregate with *GRN*-associated FTLD (Van Deerlin *et al*, 2010). *TMEM106B* risk variants are also associated with *C9orf72* repeat mutations (van Blitterswijk *et al*, 2014; Gallagher *et al*, 2014), TDP-43 pathology, severity of *GRN* independent FTLD, and other neurodegenerative disorders (Rutherford *et al*, 2012; Murray *et al*, 2014; Nelson *et al*, 2015; Yu *et al*, 2015). The most significant SNPs are in high linkage disequilibrium with a SNP that leads to a threonine to serine exchange at amino acid 185. The minor protective S185 allele is underrepresented in FTLD and may thus reduce the risk of *GRN* mutation carriers (Cruchaga *et al*, 2011; Finch *et al*, 2011; van der Zee *et al*, 2011). However, contradictory findings make it difficult to understand how TMEM106B and PGRN functionally interact to increase the risk for FTLD-TDP. There is some evidence that the risk haplotype enhances inflammatory gene expression (Rhinn & Abeliovich, 2017; Ren *et al*, 2018), whereas the protective variant provides neuroprotection (Li *et al*, 2020). Functionally, TMEM106B is linked to the lysosomal protein degradation pathway and autophagy suggesting an interaction with similar functions of PGRN. TMEM106B is an endo-lysosomal type 2 transmembrane protein and plays a crucial role in regulating lysosomal size, morphology, subcellular trafficking, and acidification (Chen-Plotkin *et al*, 2012; Lang *et al*, 2012; Brady *et al*, 2013; Schwenk *et al*, 2014; Stagi *et al*, 2014). In neurons, TMEM106B overexpression leads to enlarged lysosomes, inhibits their acidification and transport, and results in accumulation of LAMP1-positive structures at the cell soma (Stagi *et al*, 2014). This may be in line with increased mRNA and protein levels (Van Deerlin *et al*, 2010; Nicholson *et al*, 2013; Gallagher *et al*, 2017) in FTLD-TDP patients (Van Deerlin *et al*, 2010; Chen-Plotkin *et al*, 2012; Gotzl *et al*, 2014). This would also be consistent with the observation that a *Tmem106b* knockout rescues lysosomal deficits in *Grn* knockout mice (Klein *et al*, 2017). However, knockdown of TMEM106B also results in clustering of lysosomes in nuclear proximity and enhanced retrograde transport in dendrites (Schwenk *et al*, 2014; Clayton *et al*, 2018). Moreover, similar to TMEM106B overexpression, TMEM106B deficiency in mice also results in impaired lysosomal acidification and reduced lysosomal enzyme activities (Klein *et al*, 2017; Arrant *et al*, 2018) and altered axonal transport accompanied by accumulation of lipofuscin and autophagosomes (Luningschror *et al*, 2020). Thus, it is currently unclear if a loss or a gain of function contributes to the elevated risk for FTLD.

To understand a potential pathological consequence and synergistic effects of PGRN and TMEM106B loss of function, we investigated single knockout and double knockout animals. Surprisingly, we found that loss of TMEM106B strongly enhanced age-related PGRN phenotypes resulting in robust TDP-43 pathology, early lysosomal dysfunction accompanied by an accumulation of ubiquitinated proteins, severe microgliosis/astrogliosis, and dramatically reduced life span. This suggests that the *TMEM106B* risk alleles may modulate *GRN*-associated FTLD via a loss-of-function mechanism.

Results

Loss of PGRN and TMEM106B leads to early motor deficits in mice

To understand the contribution of a loss of function of TMEM106B to FTLD pathology, we generated *Grn/Tmem106b* double knockout animals. The *Tmem106b*$^{-/-}$ mouse line was generated by injection of targeted ES cells (KOMP clone EPD0047_1_E02) into BALB/C blastocysts. Germline transmission of the tm2a allele (Wtsi lacZ genetrap "knockout first" cassette between exon3 and exon4) was verified, and the mice were bred with constitutively *Cre* recombinase expressing mice to delete exon 4 and generate the *Tmem106b*$^{-/-}$ (tm2b) founder generation (Fig 1A) (see also (Luningschror *et al*, 2020)). *Grn*$^{-/-}$/*Tmem106b*$^{-/-}$ mice were generated by crossing *Tmem106b*$^{-/-}$ mice with *Grn*$^{-/-}$ mice (Kayasuga *et al*, 2007). All genotypes were verified by Western blotting (Fig 1B). In contrast to the single knockout lines, double knockout *Grn*$^{-/-}$/*Tmem106*b$^{-/-}$ mice showed a reduced life expectancy. According to animal welfare practices, we had to sacrifice these mice at 16–18 weeks of age when they reached pre-defined endpoint criteria. The hind-leg clasping reflex test revealed an overt phenotypic difference between 3-month-old *Grn*$^{-/-}$/*Tmem106b*$^{-/-}$ mice and single knockout littermates or wild-type (WT) mice. *Grn*$^{-/-}$/*Tmem106b*$^{-/-}$ mice showed sustained hind limb clasping associated with trunk flexion while single knockout and WT mice held their

Figure 1. Early motor deficits in *Grn*$^{-/-}$/*Tmem106b*$^{-/-}$ mice.

A Schema of the mouse wild-type and mutant *Tmem106b* locus. The *tm2a* allele carries a *LacZ-Neo* selection cassette in intron 3 and a loxP-flanked exon 4. Upon *Cre* recombinase expression in the germline, exon 4 is deleted and *Tmem106b* expression abolished (*tm2b allele*).

B Western blot analysis of total brain lysates of wild-type, *Tmem106b*$^{-/-}$, *Grn*$^{-/-}$ and *Grn*$^{-/-}$/*Tmem106b*$^{-/-}$ mice using antibody 6F2 to detect TMEM106B. (4.5-month-old mice with the given genotype; $n = 3$ biological replicates per genotype).

C Hind limb clasping test wild-type, *Tmem106b*$^{-/-}$, *Grn*$^{-/-}$, *Grn*$^{+/-}$/*Tmem106b*$^{-/-}$ and *Grn*$^{-/-}$/*Tmem106b*$^{-/-}$ mice. Representative pictures are shown of three mice analyzed for each genotype at 3 months of age.

D Rotarod performance of wild-type, *Tmem106b*$^{-/-}$, *Grn*$^{-/-}$, *Grn*$^{+/-}$/*Tmem106b*$^{-/-}$ and double knockout animals at 3–4 months of age. Number of animals used for analysis, 10 wild-type, 12 *Tmem106b*$^{-/-}$, five *Grn*$^{-/-}$, seven *Grn*$^{+/-}$/*Tmem106b*$^{-/-}$, three *Grn*$^{-/-}$/*Tmem106b*$^{-/-}$ mice.

E Representative picture of a 4.5-month-old double knockout (*Grn*$^{-/-}$/*Tmem106b*$^{-/-}$) mouse after manual flip.

Data information: For statistical analysis (D), one-way ANOVA with Tukey's *post hoc* test was used to compare the mean ± SD of the individual genotypes. Significance is indicated; *$P < 0.05$; **$P < 0.01$; and ****$P < 0.0001$.
Source data are available online for this figure.

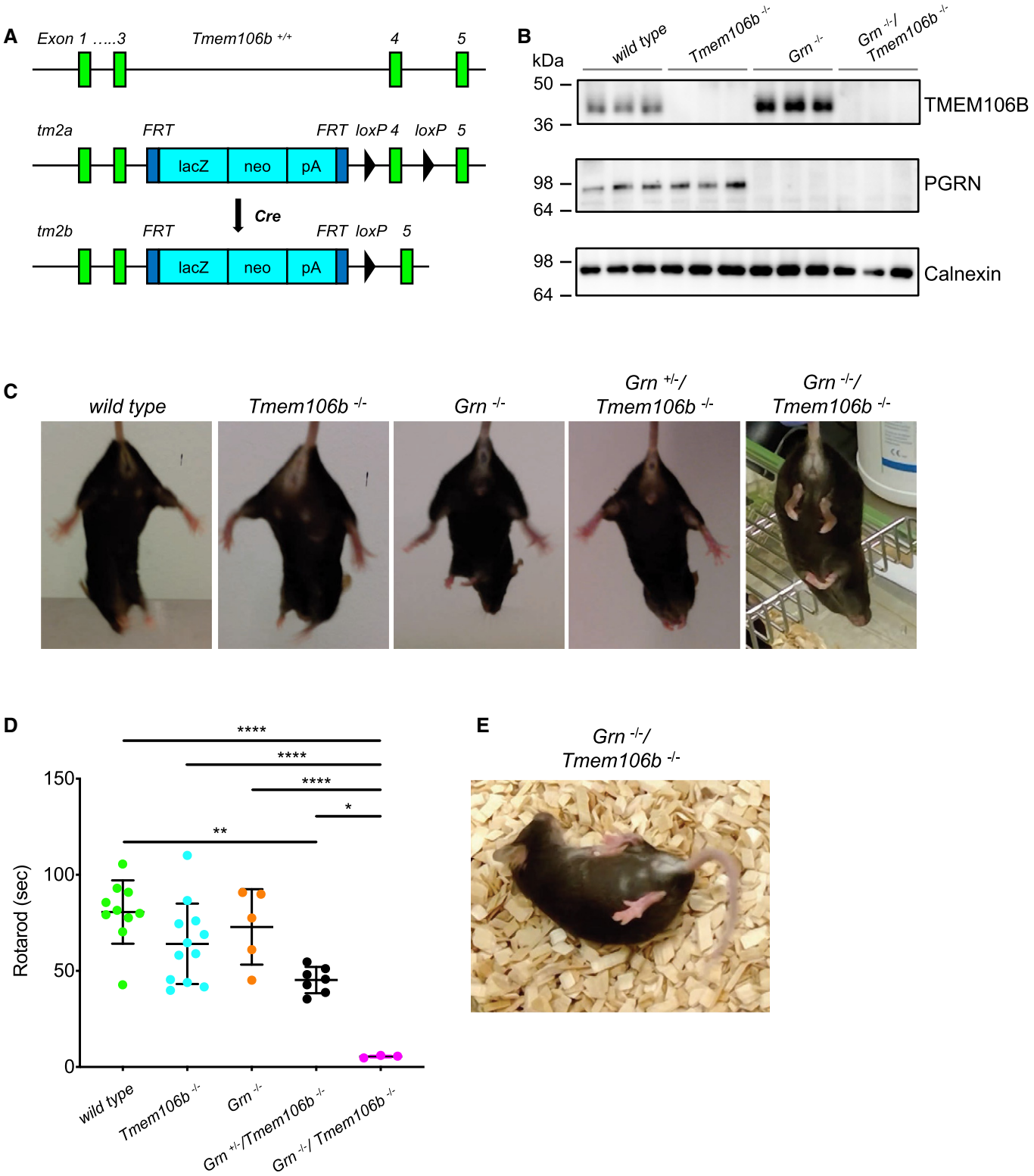

Figure 1.

hind limbs apart with paw external rotation (Fig 1C). Furthermore, the rotarod test confirmed motor incoordination in $Grn^{-/-}/Tmem106b^{-/-}$ mice (Fig 1D). The motor deficits of the $Grn^{-/-}/Tmem106b^{-/-}$ mice, visible by shaking-like movements and paresis of hind limbs, increased with age to a stage in which the mice could not turn back, when they were manually flipped over (Fig 1E and Movie EV1). To investigate whether the total loss of TMEM106B and PGRN is required for developing such a strong phenotype, we analyzed $Grn^{-/+}/Tmem106b^{-/-}$ mice. Although the hind-leg clasping reflex was normal (Fig 1C) and the mice could not be turned on

their back, rotarod performance was significantly impaired compared to WT but significantly improved compared to double knockout mice (Fig 1D). Thus, reduced PGRN levels in combination with TMEM106B loss of function exacerbate the rather mild phenotypes of the individual knockouts. However, the strong effect on life expectancy only occurred upon total loss of both proteins PGRN and TMEM106B.

Enhanced dysregulation of genes in the double knockout is associated with microglia and astrocyte function

To specify functional changes in $Grn^{-/-}/Tmem106b^{-/-}$ mice, we analyzed the expression of genes associated with neurodegenerative diseases using the nCounter® Neuropathology panel (NanoString Technologies) in total brain of 4.5-month-old mice. Genes expressed in neurons, astrocytes, microglia, oligodendrocytes, and endothelial cells, addressing six fundamental themes of neurodegeneration including neurotransmission, neuron–glia interaction, neuroplasticity, cell structure integrity, neuroinflammation, and metabolism, were analyzed. Gene expression levels of 760 genes in each sample were normalized against the geometric mean of 10 housekeeping genes. The most significant dysregulation of genes was found in $Grn^{-/-}/Tmem106b^{-/-}$ mice (Fig 2A–C). While in single knockout mice expression of genes was altered no more than two-fold up or 0.5-fold down, in the double knockout mice 23 genes were dysregulated above/below these values. Overlap in gene expression was considered if a gene was significantly changed in the respective mouse models with more than 20% change in at least one mouse model. Most overlap exists between $Tmem106b^{-/-}$ and $Grn^{-/-}/Tmem106b^{-/-}$ mice (15 genes, 10 up, five down), while the strongest modulation occurs in a gene cluster associated with activated microglia in $Grn^{-/-}$ and $Grn^{-/-}/Tmem106b^{-/-}$ mice (Cd68, C1qc) or in all three mouse models (Trem2, C1qa, C1qb; Fig 2D). Notably, almost all overlapping genes are regulated in the same direction. The double knockout mice show the strongest effects, and the changes in gene expression are not simply the additive effects of single knockout mice (Fig 2D). In line with previous findings, pathway analyses revealed upregulation of gene clusters associated with activated microglia, autophagy (Lui *et al*, 2016; Gotzl *et al*, 2019), and angiogenesis in $Grn^{-/-}$ mice and in $Tmem106b^{-/-}$ mice (Fig 2E). Scores of these gene clusters were strongly elevated in the double knockout animals (Fig 2E), suggesting severe microgliosis and deficits in protein degradation. Moreover, all downregulated genes in $Grn^{-/-}/Tmem106b^{-/-}$ mice are associated with "axon and dendrite structure" and "neural connectivity". The strongest downregulation in $Grn^{-/-}/Tmem106b^{-/-}$ mice was observed for genes affecting "myelination" (Fa2h, Mog, Mag, Ugt8a, Mal; Fig 2C). Note that downregulation of myelination-associated genes could be confirmed on the protein level (Fig EV1). Interestingly, in several pathways associated with neuronal function like "neuronal cytoskeleton", "myelination", "axon and dendrite structure", and "vesicle trafficking", a high score is only observed in double knockout mice, while single knockout mice show no changes (Fig 2E).

Besides upregulated genes associated with hyperactivated microglia, Gfap is 6.5-fold upregulated and therefore after Cd68, which is eight-fold upregulated, the second strongest upregulated gene in the double knockout mice (Fig 2C). Thus, we also addressed glial pathology by analyzing gene expression using the nCounter® Neuroinflammation panel (NanoString Technologies) covering 757 genes and 13 housekeeping in total brain of 4.5-month-old mice. Gene expression levels were analyzed as described for the nCounter® Neuropathology panel. As expected expression changes in the single knockout mice are low, no gene reaches a two-fold or 0.5-fold change in expression (Fig 3A and B). The double knockout mice show again the strongest effects with 27 genes either with a two-fold or 0.5-fold change, and 126 genes with more than 20% change (Fig 3C). Changes in gene expression are not simply additive (Fig 3D). Ninteen genes were altered in all three mouse models and 17 genes altered in the double knockout together with either single knockout (Fig 3D). As observed for the Neuropathology panel, almost all overlapping genes are regulated in the same direction. Downregulation overlapped only in $Tmem106b^{-/-}$ and $Grn^{-/-}/Tmem106b^{-/-}$ mice, while upregulation overlapped more between $Grn^{-/-}$ and $Grn^{-/-}/Tmem106b^{-/-}$ mice in astrocytic and microglial expressed genes (Fig 3D). Furthermore, all inflammation-associated pathways, like "innate and adaptive", "immune response", "inflammatory signaling", and "astrocyte and microglia function", were slightly upregulated in $Grn^{-/-}$ mice and strongly increased in $Grn^{-/-}/Tmem106b^{-/-}$ mice (Fig 3E). Thus, the hyperactivated microglial state identified in the Neuropathology panel was confirmed with the Neuroinflammation panel. In line with expression changes of genes associated with myelination, detected in the Neuropathology panel,

Figure 2. Expression analysis reveals global dysregulation of gene clusters associated with autophagy and microglial activation in double knockout mice.

A–C Volcano plot of differentially expressed brain mRNAs of 4.5-month-old mice (n = 3 biological replicates per genotype) detected by the Neuropathology panel of NanoString. Expression changes were only taken into consideration when the extent of change was above 20% as indicated by vertical lines for all volcano plots. Gliosis- and myelination-related genes are highlighted if changes are above 20%. Fold changes are displayed after $\log_2$ transformation. (A) Comparison of differentially expressed brain mRNAs from $Tmem106b^{-/-}$ and wild-type mice. From 680 detected genes, 21 are significantly upregulated, while 10 are significantly reduced. (B) Comparison of $Grn^{-/-}$ and wild-type mice. From 680 detected genes, 12 are significantly upregulated, while six are significantly reduced. (C) Volcano plot for $Grn^{-/-}/Tmem106b^{-/-}$ and wild-type mice. From 680 detected genes, 79 are significantly upregulated, while 24 are significantly reduced.

D Display of differently expressed genes overlapping between the analyzed genotypes from (A–C). Overlap was considered if a gene was significantly changed in the respective mouse models with more than 20% change in at least one mouse model. Note that nine genes are significantly altered in all three genotypes in comparison to the wild type. Seven genes are exclusively overlapping between the $Grn^{-/-}$ and the $Grn^{-/-}/Tmem106b^{-/-}$ mice. $Tmem106b^{-/-}$ and $Grn^{-/-}/Tmem106b^{-/-}$ mice share 15 significantly altered genes. $Tmem106b^{-/-}$ and $Grn^{-/-}$ mice share one significant altered gene. Data represent the mean ± SD.

E Gene set analysis based on NanoString advanced analysis R-script included in the Neuropathology panel.

Data information: For statistical analysis of volcano plot data, unpaired two-tailed Student's t-test was performed between individual genotypes and the wild-type control condition. Significance was accepted when $P < 0.05$ as indicated by the dotted line.
Source data are available online for this figure.

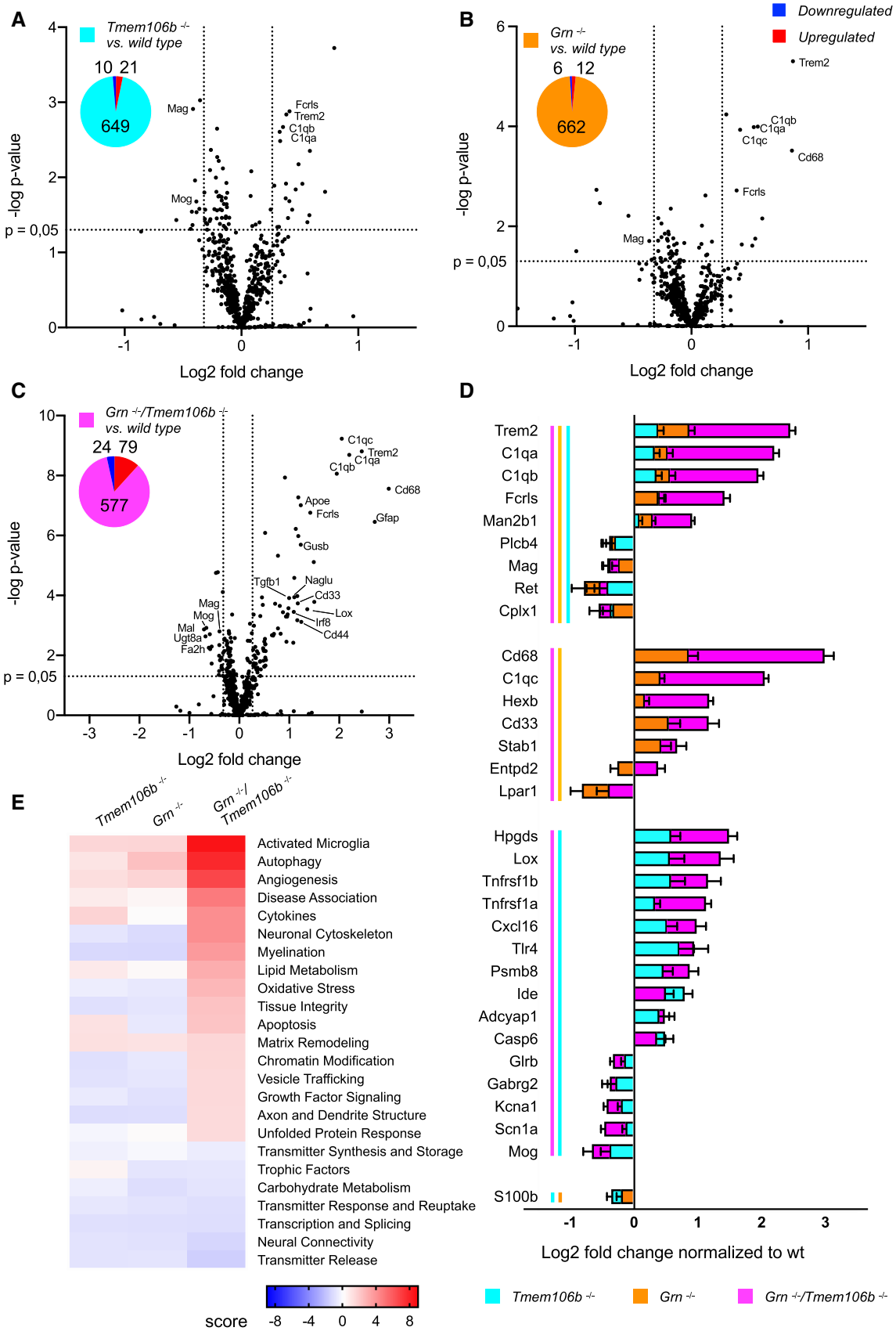

Figure 2.

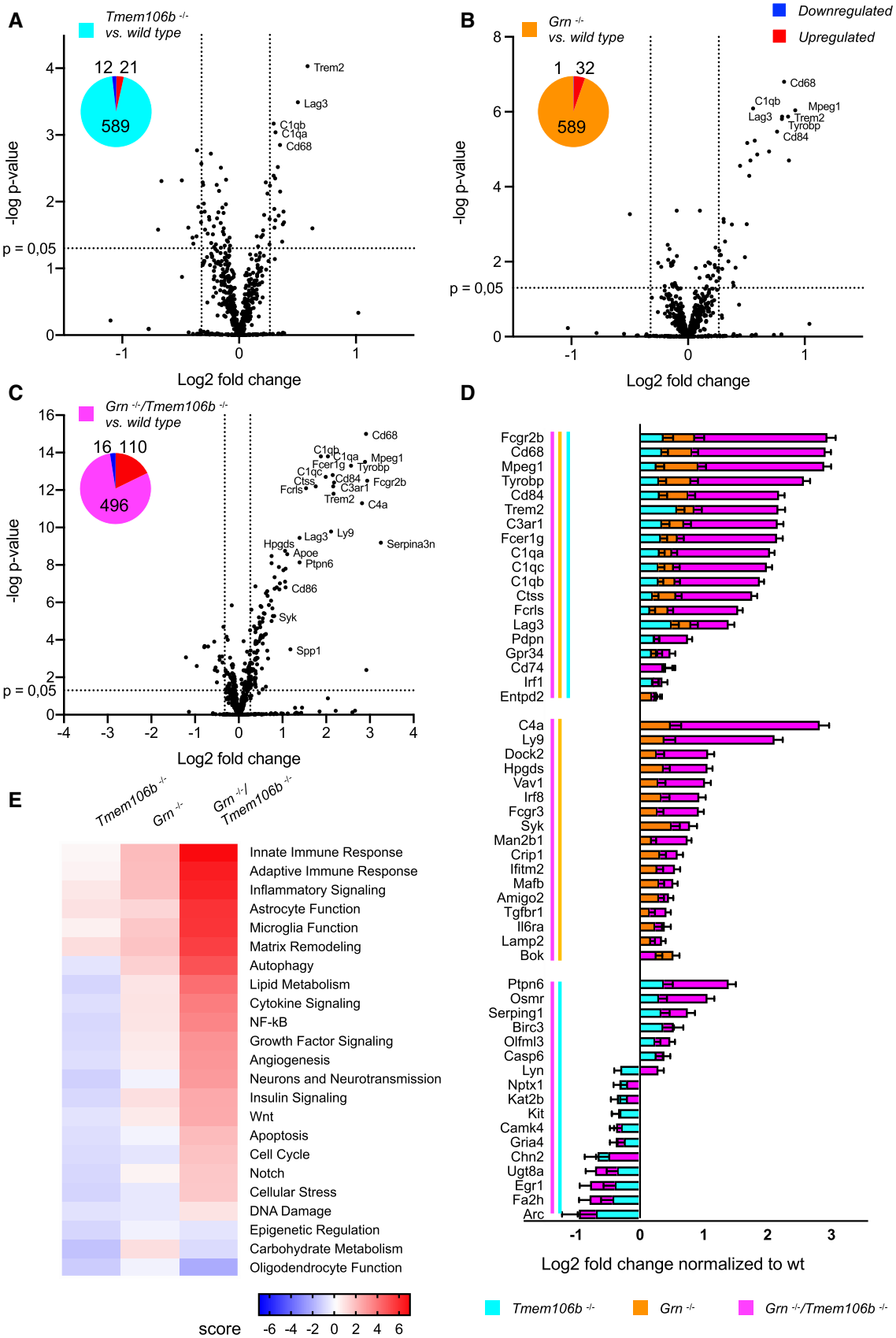

Figure 3.

Figure 3. Expression analysis reveals enhanced dysregulation of genes associated with microglia and astrocyte function.

A–C Analysis of brain mRNA expression of 4.5-month-old mice (five wild-type, four $Grn^{-/-}$, four $Tmem106b^{-/-}$, five $Grn^{-/-}/Tmem106b^{-/-}$ mice) detected by the Neuroinflammation panel by NanoString. Expression changes were only taken into consideration when the extent of change was above 20% as indicated by vertical lines for in all volcano plots. Gliosis-related genes are highlighted if changes are above 20%. Fold changes are displayed after $\log_2$ transformation. (A) Comparison of differentially expressed mRNA of $Tmem106b^{-/-}$ mice in comparison to wild-type mice. From 622 detected genes, 21 are significantly upregulated, while 12 are significantly reduced. (B) Comparison of differentially expressed mRNA in $Grn^{-/-}$ and wild-type mice. From 622 detected genes, 32 are significantly upregulated, while only one is significantly reduced. (C) Volcano plot of differentially expressed brain mRNAs from $Grn^{-/-}/Tmem106b^{-/-}$ mice in comparison to wild-type mice. From 622 detected genes, 110 are significantly upregulated, while 16 are significantly reduced.

D Display of differently expressed genes overlapping between the analyzed genotypes from (A–C). Overlap was considered if a gene was significantly changed in the respective mouse models with more than 20% change in at least one mouse model. Note that 19 genes are significantly altered in all three genotypes in comparison to the wild type. Seventeen genes are exclusively overlapping between the $Grn^{-/-}$ and the $Grn^{-/-}/Tmem106b^{-/-}$ mice. $Tmem106b^{-/-}$ and $Grn^{-/-}/Tmem106b^{-/-}$ mice share 17 significantly altered genes. Data represent the mean ± SD.

E Gene set analysis based on NanoString advanced analysis R-script included in the Neuroinflammation panel.

Data information: For statistical analysis of volcano plot data, unpaired two-tailed Student's *t*-test was performed between individual genotypes and the wild-type control condition. Significance was accepted when $P < 0.05$ as indicated by the dotted line.
Source data are available online for this figure.

"oligodendrocyte function" is also strongly reduced in the double knockout (Fig 3E).

Exaggerated gliosis in young $Grn^{-/-}/Tmem106b^{-/-}$ mice

To validate the changes of the mRNA signature at the protein level, we performed biochemical analyses of total brain homogenate from 4.5-month-old mice. This confirmed a significant 3.4- to 4.7-fold increase of GFAP and IBA1 expression in $Grn^{-/-}/Tmem106b^{-/-}$ mice (Fig 4A and B) which is in line with strong astrogliosis and microgliosis in the double knockout. Importantly and consistent with our previous findings in $Grn^{-/-}$ mice (Gotzl *et al*, 2014), at this age no microgliosis and astrogliosis was apparent in the single knockouts (Fig 4A and B). Next, we investigated by immunohistochemistry which brain regions were particularly affected by gliosis. Astrogliosis and microgliosis were most prominent in the thalamus, pons and medulla, midbrain, cerebellum, and cerebral cortex of the double knockout mice (Figs 4C and D, and EV2A and B). To confirm enhanced microgliosis in double knockout mice *in vivo*, we performed previously established TSPO-μPET (Brendel *et al*, 2016; Gotzl *et al*, 2019). A higher increase of TSPO signals between 2- and 3.5-month-old $Grn^{-/-}/Tmem106b^{-/-}$ mice compared to WT was detected in the regions of accelerated astro- and microgliosis, like thalamus, pons and medulla, midbrain, and cerebellum (Fig 4E). To further investigate microglial activation in the different mouse lines, we analyzed protein expression of CD68, CLEC7A, TREM2, and ApoE in total brain extracts of 4.5-month-old mice (Fig 5A). Quantification revealed a significant increase of all four proteins in $Grn^{-/-}/Tmem106b^{-/-}$ mice (Fig 5B). Only TREM2 was also significantly elevated in $Grn^{-/-}$ mice (Fig 5B). In $Grn^{-/-}/Tmem106b^{-/-}$ mice, most IBA1-positive microglia are also positive for CLEC7A, CD68, and to a lower extent for TREM2 confirming activated microglia already at the age of 4.5 months (Fig 5C–E).

The strong motor phenotype together with the gliosis in regions of the brainstem let us additionally analyze the spinal cord for astrogliosis and microgliosis. Again, only $Grn^{-/-}/Tmem106b^{-/-}$ mice show a strongly increased expression of GFAP and CD68, a microglial lysosomal membrane protein, in both white and gray matter (Fig EV3).

Enhanced lysosomal and autophagic dysfunction in $Grn^{-/-}/Tmem106b^{-/-}$ mice

Activation of microglia is accompanied by elevated expression of lysosomal cathepsins, which was described for aged $Grn^{-/-}$ mice (Ahmed *et al*, 2010; Wils *et al*, 2012; Tanaka *et al*, 2013; Gotzl *et al*, 2014; Klein *et al*, 2017). In line with these observations, $Grn^{-/-}/Tmem106b^{-/-}$ mice show elevated levels of the cathepsin D, cathepsin B, and cathepsin L compared to WT and single knockout mice (Fig 6A and B). The elevated CatD and CatL expression levels result in significantly increased enzymatic activities compared to WT and single knockout mice (Fig 6C). Elevated lysosomal protease expression and lysosomal activity often indicate impaired protein degradation and accumulation of autophagy cargo as observed in NCL mouse models (Gotzl *et al*, 2014) and in aged *Grn* knockout mice (Ahmed *et al*, 2010; Wils *et al*, 2012; Gotzl *et al*, 2014). Furthermore, autophagy is among the strongest hits in the pathway analysis

Figure 4. Astrogliosis and microgliosis in different brain regions of $Grn^{-/-}/Tmem106b^{-/-}$ mice.

A Western blot analysis of GFAP and IBA1 in total brain lysates from 4.5-month-old mice with the given genotype ($n = 3$ biological replicates per genotype).

B Quantification of (A). Protein expression was normalized to levels in wild-type animals. Data represent the mean ± SD.

C Expression of GFAP in sagittal brain sections. Representative images of indicated brain regions (CBX, cerebellum; CTX, cortex; MY, medulla; TH, thalamus). Scale bar indicates 100 μm.

D Expression of IBA1 in sagittal brain sections. Representative images of indicated brain regions (CBX, cerebellum; CTX, cortex; MY, medulla; TH, thalamus). Scale bar indicates 100 μm.

E *In vivo* ^{18}F-GE180 TSPO μPET imaging. Two female $Grn^{-/-}/Tmem106b^{-/-}$ and five female wild-type mice underwent longitudinal TSPO μPET at 2.0 and 3.5 months of age. All analyses were performed by PMOD (V3.5, PMOD technologies). Normalization of injected activity was performed by the previously validated myocardium correction method.

Data information: (B), one-way ANOVA with Tukey's *post hoc* test was used to compare individual genotypes. Significance is indicated; ***$P < 0.001$; and ****$P < 0.0001$.
Source data are available online for this figure.

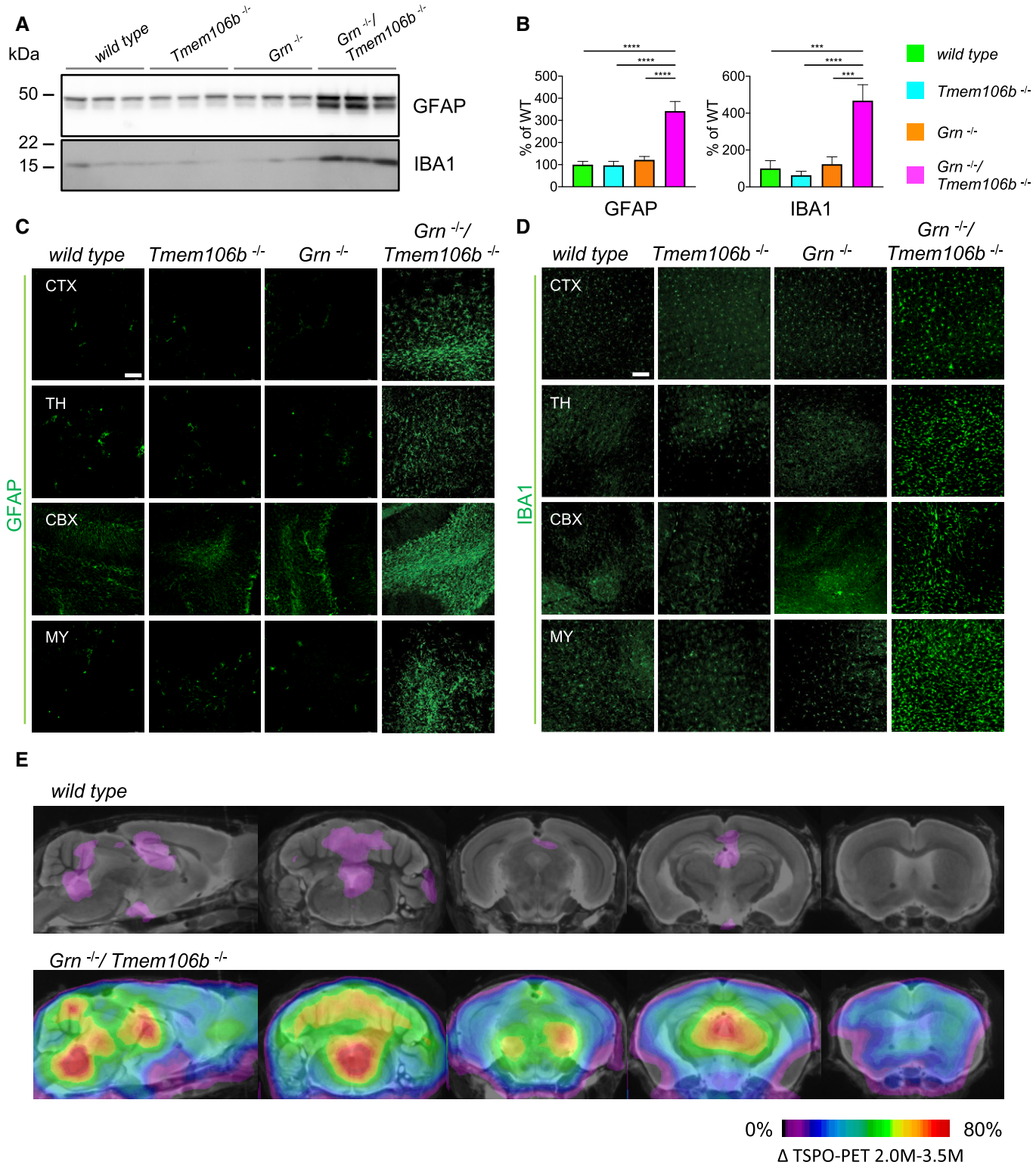

Figure 4.

of both NanoString panels (Figs 2E and 3E); therefore, we next investigated accumulation of autophagic cargo. Since the complete loss of PGRN results in a NCL-like storage phenotype with exaggerated deposition of lipofuscin in aged mice (Kleinberger *et al*, 2013), we investigated the autofluorescence signal in single and double knockout mice. Lipofuscin is detectable predominantly in the thalamus of the double knockout mice, while the single knockout mice show weak (*Tmem106b*$^{-/-}$) or no lipofuscin deposition (*Grn*$^{-/-}$) at

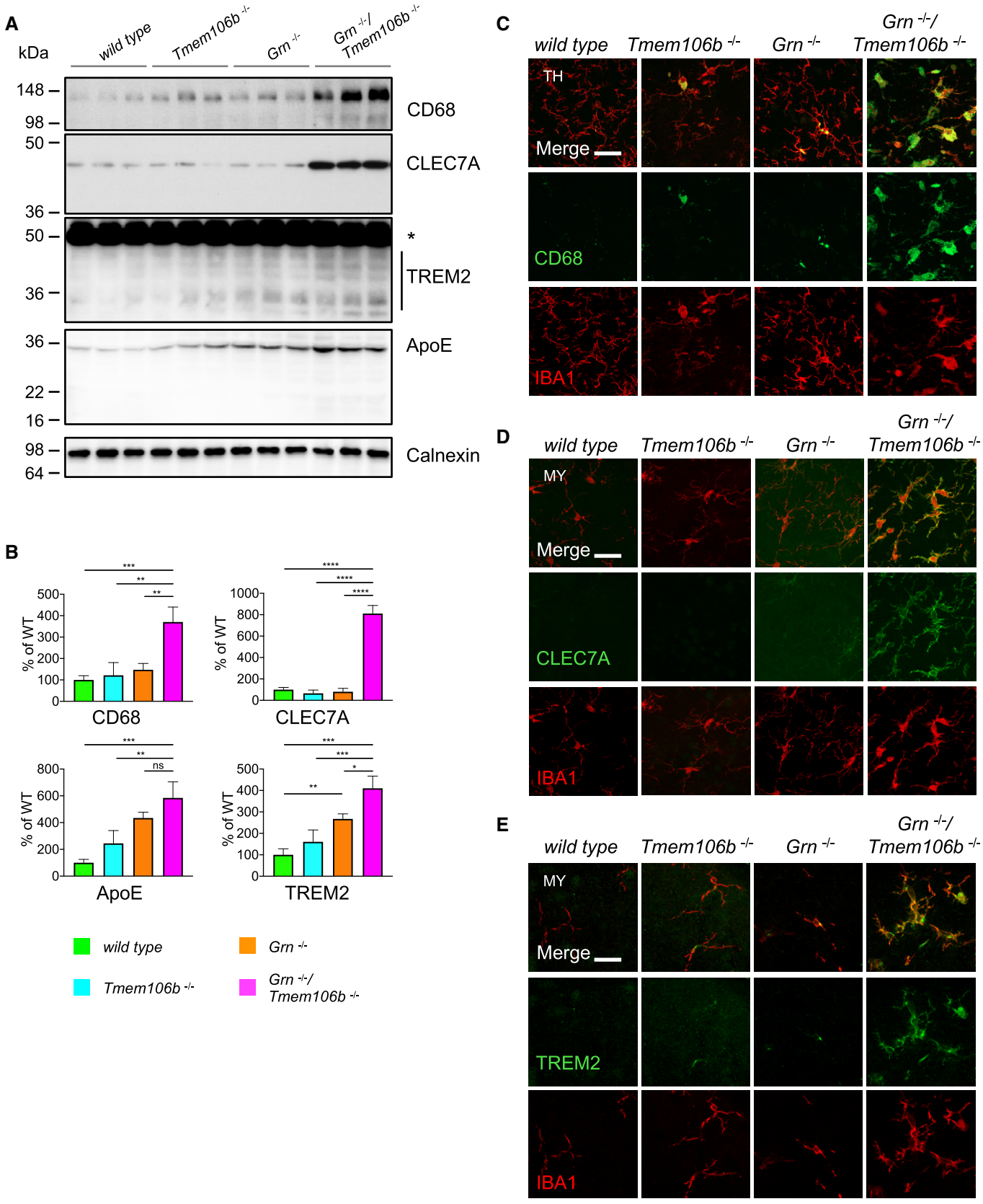

Figure 5.

Figure 5. Enhanced expression of proteins associated with activated microglia in $Grn^{-/-}/Tmem106b^{-/-}$ mice.

A Western blot analysis of CD68, CLEC7A, TREM2, and ApoE in total brain lysates from 4.5-month-old mice with the given genotype. Asterisk indicates unspecific band (n = 3 biological replicates per genotype).

B Quantification of (A). Protein expression was normalized to levels in wild-type animals. Data represent the mean ± SD.

C Expression of CD68 and the microglial marker IBA1 in sagittal brain sections. Representative images of indicated brain regions (TH, thalamus). Scale bar indicates 25 μm.

D Expression of CLEC7A and the microglial marker IBA1 in sagittal brain sections. Representative images of indicated brain regions (MY, medulla). Scale bar indicates 25 μm.

E Expression of TREM2 and the microglial marker IBA1 in sagittal brain sections. Representative images of indicated brain regions (MY, medulla). Scale bar indicates 25 μm.

Data information: For statistical analysis of protein levels (B), one-way ANOVA with Tukey's *post hoc* test was used to compare individual genotypes. Significance is indicated; *$P < 0.05$; **$P < 0.01$; ***$P < 0.001$; and ****$P < 0.0001$.
Source data are available online for this figure.

4.5 months of age (Fig 7A). Interestingly, in $Grn^{-/-}/Tmem106b^{-/-}$ mice lipofuscin accumulation partially overlaps with the microglia marker IBA1, which may suggest early degradation deficits in microglia (Fig 7A). Lipofuscin accumulation indicates a dysfunction in protein degradation as described for NCL (Palmer *et al*, 2013) and *GRN*-associated FTLD (Ward *et al*, 2017). Since protein aggregates and long-lived proteins are normally cleared by autophagy, we investigated the multifunctional adaptor protein p62/sequestosome1 (p62/SQSTM1), which directs ubiquitinated cargos for autophagy. Indeed, $Grn^{-/-}/Tmem106b^{-/-}$ mice show robustly elevated p62/SQSTM1 levels in RIPA and urea lysates compared to single knockout and WT mice (Fig 7B and C). The accumulation of p62/SQSTM1 in the urea lysate reflects reduced solubility and indicates elevated protein aggregation. Furthermore, p62/SQSTM1 accumulates in all brain regions associated with elevated astrogliosis and microgliosis of $Grn^{-/-}/Tmem106b^{-/-}$ mice including the spinal cord (Figs 7D and EV3). Co-staining of p62/SQSTM1 with NeuN, Iba1, or GFAP shows that most p62/SQSTM1 accumulates in neurons and not in microglia or astrocytes (Figs 7E and F). The minor co-localization of p62 with microglia is also supported by little overlay in the cerebellar staining (Fig EV4). In line with accumulation of the p62/SQSTM1, ubiquitinated proteins are significantly increased and autophagosomes are accumulated, as indicated by elevated LC3II levels, in double knockout mice compared to single knockout mice (Fig 7B and C).

Accelerated TDP-43 aggregation and phosphorylation in $Grn^{-/-}/Tmem106b^{-/-}$ mice

The pathological hallmarks of *GRN*-associated FTLD are nuclear and cytoplasmic, ubiquitin positive inclusions composed of phosphorylated TDP-43 and its proteolytically generated C-terminal fragments. In aged *Grn* knockout mice, cytoplasmic TDP-43 depositions were only occasionally detected (Guo *et al*, 2010; Kleinberger *et al*, 2010; Yin *et al*, 2010b). To address the question if the additional loss of TMEM106B promotes TDP-43 pathology in the *Grn* knockout mice, we performed immunohistochemistry. Small cytoplasmic TDP-43 inclusions were detected throughout the brain of $Grn^{-/-}/Tmem106b^{-/-}$ mice (Figs 8A and EV5). They were less frequent in the cortex and most abundant in the midbrain (Fig 8A). Some of the inclusions also contain TDP-43 phosphorylated at amino acids 409/410, a specific hallmark of FTLD-TDP (Hasegawa *et al*, 2008; Neumann *et al*, 2009) (Fig 8B). Sequential high salt (HS), RIPA, and urea extraction of total brain homogenate revealed slightly reduced levels of TDP-43 holoprotein in the HS fraction of the $Grn^{-/-}/Tmem106b^{-/-}$ mice compared to WT and $Tmem106b^{-/-}$ mice (Fig 8C and D), but elevated levels of a RIPA-extracted C-terminal TDP-43 fragments of approximately 35 kDa (Fig 8C and D). Moreover, phosphorylated TDP-43, specifically detected in the urea fraction, is significantly elevated in the double knockout mice (Fig 8C and D).

Discussion

In this study, we demonstrate that the combined knockout of *Tmem106b* and *Grn* accelerates the phenotypes of the individual knockout mice suggesting that a loss of function of TMEM106B further promotes *Grn*-associated FTLD.

Motor impairment is an early and very prominent phenotype detected in $Grn^{-/-}/Tmem106b^{-/-}$ mice and to a much lesser extent in $Grn^{+/-}/Tmem106b^{-/-}$ mice already at 3 months of age (Fig 1C–E). Hind limb clasping and paralysis has been observed in a number of mouse models for neurodegenerative diseases like Alzheimer's disease, Parkinson's disease, and other tauopathies (http://www.inf

Figure 6. Elevated lysosomal enzyme levels and activity in $Grn^{-/-}/Tmem106b^{-/-}$ mice.

A Western blot analysis of cathepsin (Cat) D, B, and L in total brain lysates from 4.5-month-old mice with the indicated genotype. Different maturation variants are indicated (hc, heavy chain; p, preform; sc, single chain; n = 3 biological replicates per genotype).

B Quantification of proteolytically generated variants of cathepsin D, B, and L normalized to levels in wild-type animals from (A). Data represent the mean ± SD.

C Catalytic activity of cathepsin D, B, and L. Total brain lysates from 4.5-month-old mice were incubated with quenched fluorogenic substrate for Cat D, Cat B, and Cat L. The linear increase of fluorescence signal was measured and then normalized to wild type. Data represent the mean normalized activity ± SD (n = 3 biological replicates per genotype).

Data information: For statistical analysis of normalized data (B, C), one-way ANOVA with Tukey's *post hoc* test was used to compare individual genotypes. Significance is indicated; ns $P > 0.05$; *$P < 0.05$; **$P < 0.01$; ***$P < 0.001$; and ****$P < 0.0001$.
Source data are available online for this figure.

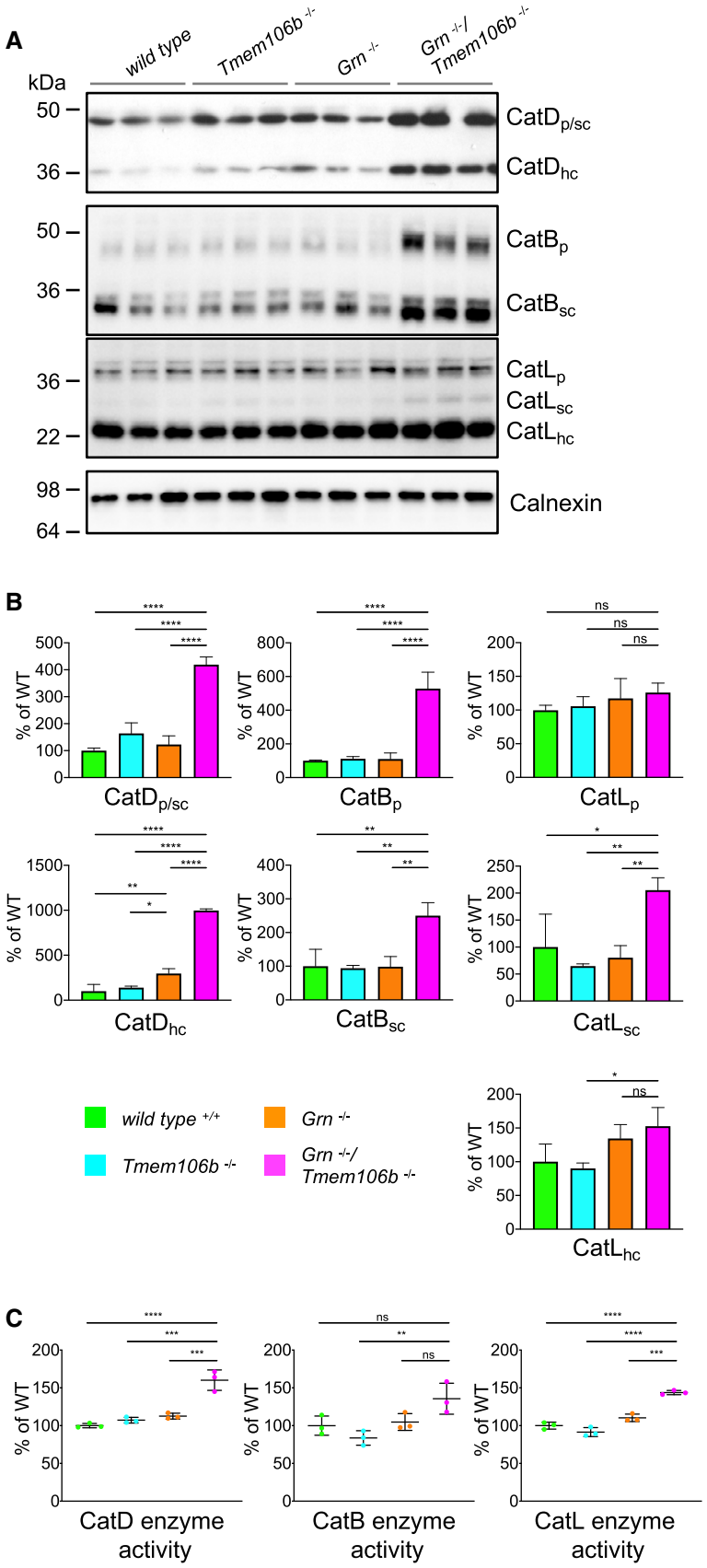

Figure 6.

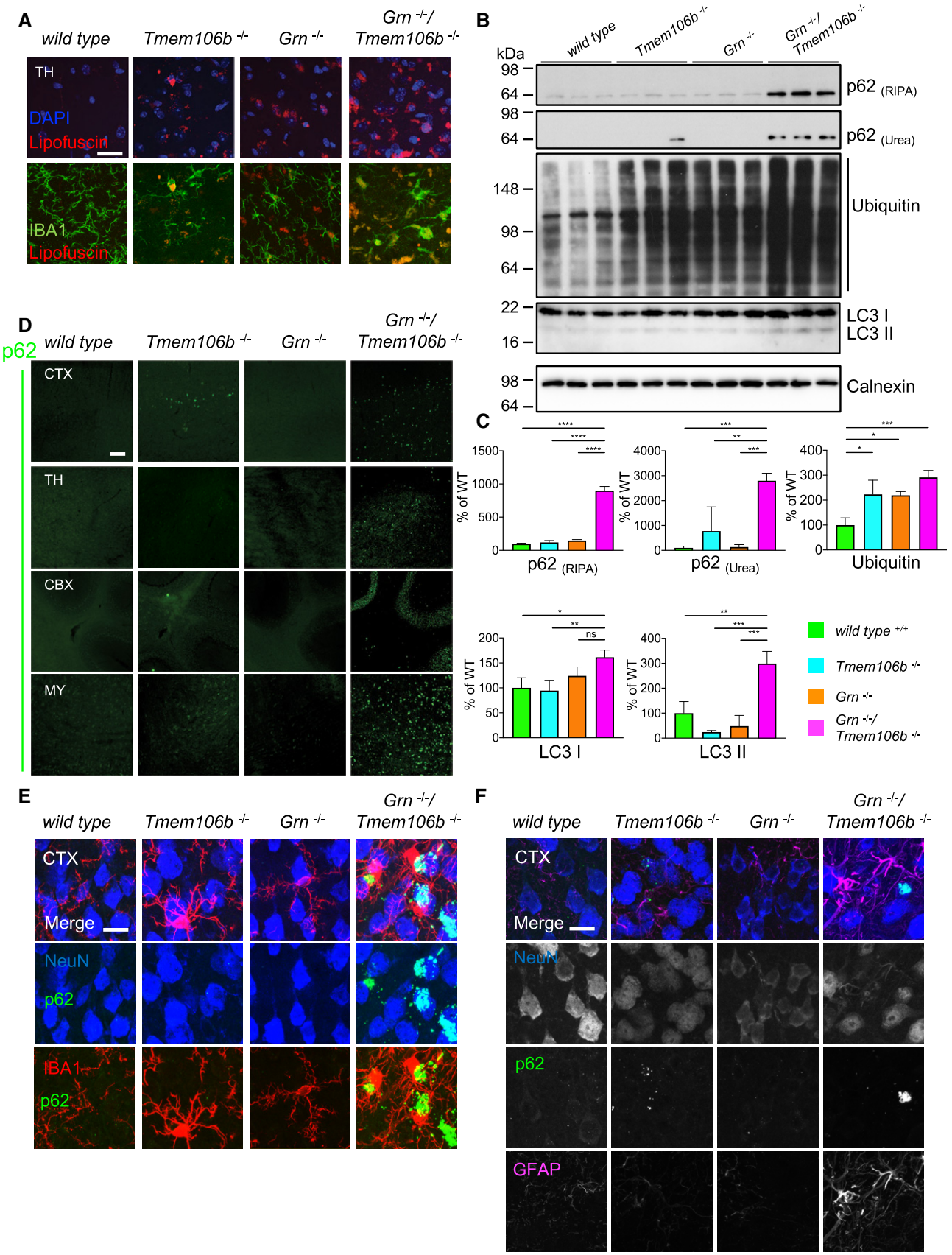

Figure 7.

Figure 7. Widespread impairment of autophagy and protein degradation in $Grn^{-/-}/Tmem106b^{-/-}$ mice.

A Immunofluorescence analysis of lipofuscin (red) and IBA1 (green) in sagittal brain sections. Representative images of the thalamus (TH). Scale bar indicates 25 μm.

B Western blot analysis of ubiquitin and the autophagy marker LC3 in RIPA, and p62 in RIPA and urea total brain lysates from 4.5-month-old mice with the indicated genotype. Calnexin used as a loading control. (n = 3 biological replicates per genotype).

C Quantification of (B). Protein expression was normalized to levels in wild-type animals. Data represent the mean ± SD.

D Immunofluorescence analysis of p62 in sagittal brain sections. Representative images of indicated brain regions (CBX, cerebellum; CTX, cortex; MY, medulla; TH, thalamus). Scale bar indicates 100 μm.

E Localization of p62 mainly in NeuN-positive cells in the cortex (CTX) of 4.5-month-old mice. Minor overlap of aggregates with microglial marker IBA1. Scale bar indicates 15 μm.

F Complete overlap of co-staining of p62 with NeuN in the cortex (CTX) and not with the reactive astrocyte marker GFAP. Scale bar indicates 15 μm.

Data information: For statistical analysis of normalized data (C), one-way ANOVA with Tukey's *post hoc* test was used to compare individual genotypes. Significance is indicated; ns $P > 0.05$; *$P < 0.05$; **$P < 0.01$; ***$P < 0.001$; and ****$P < 0.0001$.
Source data are available online for this figure.

ormatics.jax.org/mp/annotations/MP:0001513) and may indicate progression of neurodegeneration, including cerebellar ataxia. In addition, several FTD/ALS mouse models (Wils *et al*, 2010; Le *et al*, 2016; Liu *et al*, 2016) as well as autophagy-related mouse models (Komatsu *et al*, 2005; Hara *et al*, 2006) present with similar motor deficits. Impaired autophagy has been associated with many neurodegenerative diseases (Nixon, 2013) including FTD/ALS (Gotzl *et al*, 2016). In *Tmem106b* and *Grn* double knockout mice, dysfunction in the lysosomal/autophagic degradation is indicated by accumulation of lipofuscin, ubiquitinated proteins, and the cargo adaptor protein p62 (Fig 6A–E). P62 interacts with autophagic substrates and delivers them to autophagosomes for degradation. Since p62 is also degraded during this process, accumulation of p62 suggests that the turnover of autophagosomes may be delayed which is also indicated by LC3II accumulation. Elevated autophagy associated with an increase of autophagosomes and cargo adaptor proteins is unlikely since mRNA expression of autophagy initiating genes and cargo adaptors is not elevated. However, we cannot distinguish between a failure of autophagosome/lysosome fusion or lysosomal degradation of engulfed autolysosome since both would result in cargo, p62 and LC3II accumulation.

A significant contribution of dysfunctional autophagy to the prominent phenotype of the double knockout mice is further supported by "autophagy" being one of the strongest hits in the pathway analysis of the nCounter® Neuropathology gene expression panel (Fig 2E). Indicators of impaired protein degradation are also detected in single knockout mice, albeit to a much lesser extent. In line with our earlier findings (Gotzl *et al*, 2018), "autophagy" was also one of the strongest hits in the pathway analysis in $Grn^{-/-}$ mice (Fig 2E). Furthermore, in line with previous findings (Ahmed *et al*, 2010; Ghoshal *et al*, 2012; Wils *et al*, 2012; Petkau *et al*, 2016; Beel *et al*, 2017; Tanaka *et al*, 2017; Zhou *et al*, 2017a; Gotzl *et al*, 2018) $Grn^{-/-}$ mice also showed impaired protein degradation but recognizable effects occur after the age 6 months.

Besides PGRN, the lysosomal transmembrane protein TMEM106B is linked to lysosomal integrity and function (Chen-Plotkin *et al*, 2012; Lang *et al*, 2012; Brady *et al*, 2013; Schwenk *et al*, 2014; Stagi *et al*, 2014). In cell culture, loss of TMEM106B affects lysosomal positioning and trafficking (Schwenk *et al*, 2014; Stagi *et al*, 2014) leading to reduced stress resistance (Stagi *et al*, 2014). However, overexpression also results in dysfunctional and enlarged lysosomes (Chen-Plotkin *et al*, 2012; Brady *et al*, 2013; Stagi *et al*, 2014) causing a translocation of the autophagy regulation transcription factor EB (TFEB) to nuclei (Stagi *et al*, 2014). Since such prominent phenotypes were detected in cellular systems, it is surprising that some *Tmem106b* knockout mouse models revealed only minor changes in lysosomal integrity (Klein *et al*, 2017; Arrant *et al*, 2018; Nicholson *et al*, 2018). We demonstrate that 4.5-month-old *Tmem106b* knockout mice show ubiquitin accumulation and few p62-positive inclusions in cortex and cerebellum (Fig 6A and C). Additionally, it was recently demonstrated that these mice show vacuolization in thalamus and facial motor nucleus accompanied by large LAMP1-positive membrane structures (Luningschror *et al*, 2020). Mechanistically, this could be explained by an enhanced retrograde axonal transport of lysosomes followed by an accumulation of endo-/lysosomal membrane structures at the axon initial segment, which may result in reduced fusion of lysosomes with autophagosomes. Reduced fusion may lead to impaired autophagic degradation in *Tmem106b* mice (Luningschror *et al*, 2020). Therefore, the strong phenotype of the $Grn^{-/-}/Tmem106b^{-/-}$ mice could be the consequence of disturbed lysosomal (Beel *et al*, 2017; Tanaka *et al*, 2017; Zhou *et al*, 2017a) and autophagic activities (Chang *et al*, 2017) in neurons and microglia.

In clear contrast to our observations, additional loss of TMEM106B has recently been reported to protect against the FTLD-like phenotypes in $Grn^{-/-}$ mice (Klein *et al*, 2017), while our findings and those published independently by two other research teams in this issue of EMBO Reports (Feng *et al*, 2020a; Zhou *et al*, 2020a) even demonstrate prominent gliosis, premature death, and exacerbated FTLD-like pathology. Klein *et al* report an increase in several lysosomal enzymes and their activity in 2-month-old $Grn^{-/-}$ mice. These enhanced activities of lysosomal enzymes are reduced upon additional TMEM106B knockout. However, lipofuscin accumulation is not reduced, which indicates that dysfunction in protein degradation is not improved. One may speculate that the elevated lysosomal enzyme levels and activities in $Grn^{-/-}$ mice, which predominantly occur in non-microglial cells (Gotzl *et al*, 2018), could be a rescue attempt in response to the lysosomal dysfunction. Lysosomal dysfunction shows the strongest effects in microglia since these cells have the highest PGRN expression (Lui *et al*, 2016; Gotzl *et al*, 2018) and are the degradation hub in the brain. Thus, with additional loss of TMEM106B the ability to upregulate such rescue mechanisms may be lost or overcome by factors released from malfunctional microglia. In line with the idea that TMEM106B plays a role in regulating a lysosomal rescue mechanism, it has been shown that TMEM106B knockdown reduces the signaling of TFEB (Stagi *et al*, 2014), a master regulator of the lysosomal autophagic pathway (Settembre & Ballabio, 2011; Settembre *et al*, 2011).

Loss of TMEM106B in $Grn^{-/-}$ mice dramatically enhanced astrogliosis and microgliosis (Fig 4). Note, that 7- to 18-month-old $Grn^{-/-}$ mice show similar progressive astrogliosis and microgliosis (Ahmed *et al*, 2010; Yin *et al*, 2010b; Ghoshal *et al*, 2012; Petkau *et al*, 2012; Wils *et al*, 2012) but the double knockout mice develop these phenotypes already before 4.5 months of age. Furthermore,

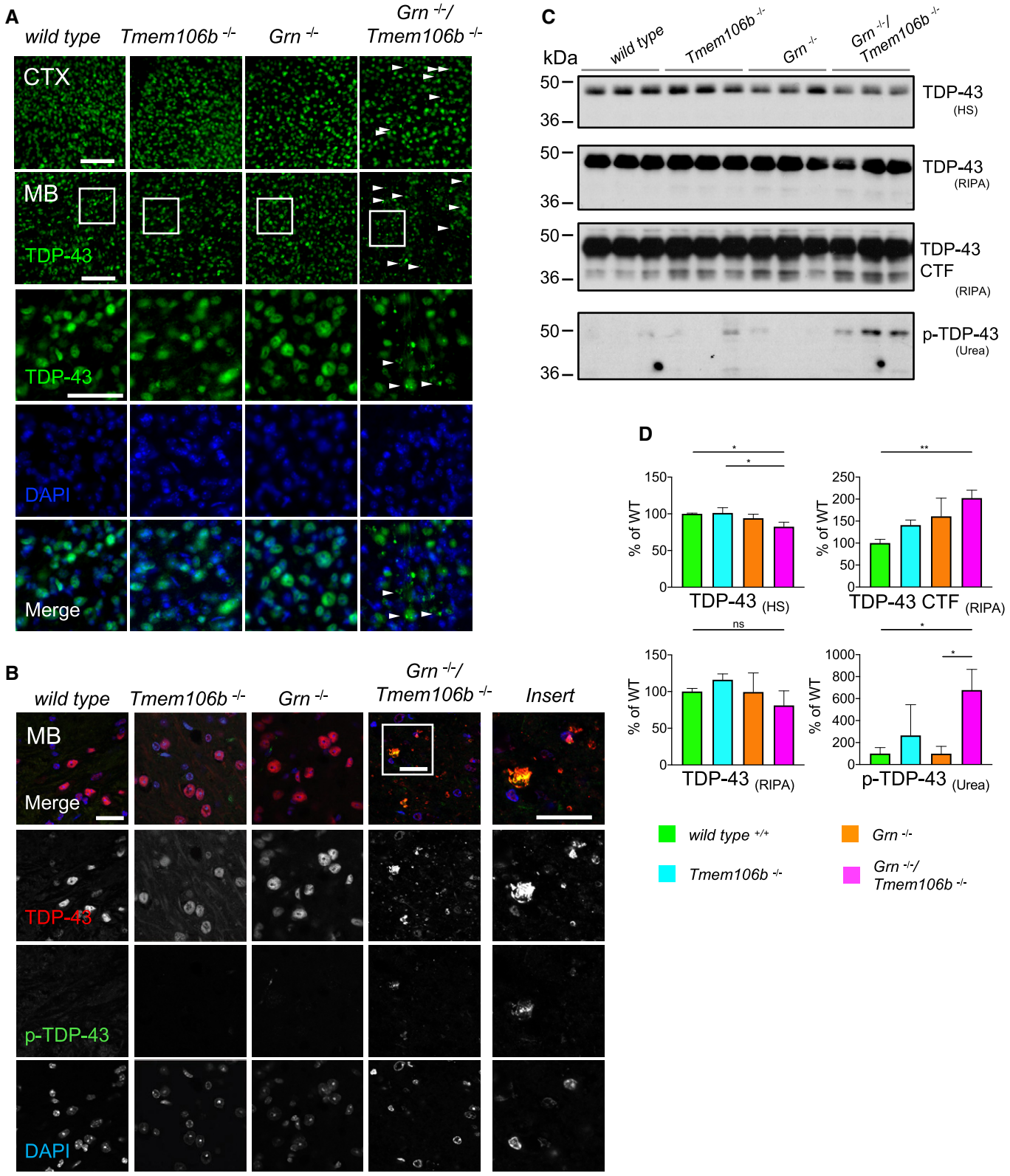

Figure 8.

Figure 8. Enhanced TDP-43 aggregation and phosphorylation in $Grn^{-/-}/Tmem106b^{-/-}$ mice.

A Immunofluorescence analysis of TDP-43 in sagittal brain sections. Representative images of indicated brain regions (CTX, cortex; MB, midbrain). White arrow heads indicate TDP-43 aggregation. Scale bar indicates 100 μm. Zoom in on TDP-43 aggregation in double knockout mouse brain sections of the midbrain, scale bar zoom in indicates 50 μm (animals 4.5 months of age).

B Immunofluorescence analysis of total TDP-43 and phosphorylated TDP-43 (p-TDP-43) in sagittal brain sections by confocal microscopy. Representative images of one confocal layer in the midbrain. Zoom in on TDP-43 aggregation in double knockout mouse brain sections of the midbrain. Scale bar indicates 25 μm (animals 4.5 months of age).

C Western blot analysis of TDP-43 and phosphorylated TDP-43 (p-TDP-43) in sequential high salt (HS)/RIPA/Urea fractionations of total brain lysates from 4.5-month-old mice with the indicated genotype. Analysis of C-terminal fragments of TDP-43 (CTF) in RIPA fraction. p-TDP-43 analyzed in Urea fraction (n = 3 biological replicates per genotype).

D Quantification of (C). Protein expression was normalized to levels in wild-type animals. Data represent the mean ± SD.

Data information: For statistical analysis of normalized data (D), one-way ANOVA with Tukey's *post hoc* test was used to compare individual genotypes. Significance is indicated; ns $P > 0.05$; *$P < 0.05$; **$P < 0.01$.

"activated microglia", "innate and adaptive immune response", "inflammatory signaling", and "astrocyte function" are the strongest hits in the gene expression pathway analysis (Figs 2E and 3E). Several genes related to inflammation and disease-associated microglia (DAM) are already slightly upregulated in the brain of $Grn^{-/-}$ mice (Figs 2B and 3B) and further increased in $Grn^{-/-}/Tmem106b^{-/-}$ mice (Figs 2C and 3C). Of note, the double knockout of $Grn^{-/-}/Tmem106b^{-/-}$ shifts the change in the mRNA signature to a much earlier time point as observed in $Grn^{-/-}$ alone (Lui *et al*, 2016; Gotzl *et al*, 2019). Among the strongest hits in double knockouts are mostly microglial expressed genes such as Cd68, Trem2, Tyrobp, Apoe, and complement factors but also genes associated with astrocyte activation such as Gfap, Serpina3n, and C4a (Figs 2C and 3C). Additionally, we detect in 4.5-month-old double knockouts reduced gene expression of myelination-associated genes (Fa2h, Mog, Mag, Ugt8a, Mal) and reduced protein levels of MOG and MAP (Fig EV1) which is in line with recent publications describing myelination deficits upon TMEM106B deficiency or loss of function (Feng *et al*, 2020b; Ikemoto *et al*, 2020; Zhou *et al*, 2020b).

Finally, the question arises how PGRN and TMEM106B deficiency results in lysosomal dysfunction affecting mainly microglia, which initiates autophagic cargo protein accumulation and pathological TDP-43 deposition in neurons. Since PGRN is mainly expressed in microglia, whereas TMEM106b is ubiquitously expressed within the brain (with the lowest expression in microglia), it is tempting to speculate that microglia lacking PGRN may initiate a pathological crosstalk to neurons. Another option would be that TMEM106B-deficient neurons required protective support from microglia, which could not be provided upon additional PGRN deficiency. In the same vein, malfunctioned oligodendrocytes may not receive support in the absence of PGRN. These scenarios suggest that dysfunctional microglia cannot appropriately communicate with other brain cells or are unable to compensate neuronal or oligodendrocyte defects.

Materials and Methods

Animal experiments

All animal experiments were performed according to German animal welfare law and approved by the government of upper Bavaria. Mice were kept under standard housing conditions including standard pellet food and water provided *ad libitum*. Recombinant mouse ES cells carrying *loxP* sites flanking *Exon 4* of *Tmem106b (tm2a allele)* were provided by the KOMP consortium (Clone EPD0047_1_E02). Blastocyst injection of the *tm2a* allele carrying ES cells leads to chimeric mice that were further bread with *Cre* deleter mice after germline transmission to obtain the $Tmem106b^{-/-}$ mouse line. The $Grn^{-/-}$ mouse line was kindly provided by Dr. M. Nishihara. Breeding and behavior tests were performed under the animal license: ROB-55.2-2532.Vet_02-17-106. Mice were perfused with PBS after deep/lethal anesthesia.

Rotarod behavior test

The rotarod test was conducted in accordance with European and national guidelines, and all experiments were performed with the researcher blinded to the genotype. The spindle speed was accelerated from 5 to 50 rpm over 5 min. The test finished either when the mouse dropped down or after the time limit of 5 min. After three rounds of training on three individual days, the average time of three trials with 1-h break in between was used.

In vivo μPET imaging

Small animal positron emission tomography (μPET) procedures followed an established standardized protocol for radiochemistry, acquisition, and post-processing (Brendel *et al*, 2016). In brief, ^{18}F-GE180 TSPO μPET with an emission window of 60–90 min post-injection was used to measure cerebral microglial activity. Two female $Grn^{-/-}$ &$Tmem106b^{-/-}$ and five female wild-type mice underwent longitudinal TSPO μPET at 2.0 and 3.5 months of age. All analyses were performed by PMOD (V3.5, PMOD technologies, Basel, Switzerland). Normalization of injected activity was performed by the previously validated myocardium correction method (Deussing *et al*, 2018). TSPO μPET estimates (percentage changes over time) deriving from a brainstem target VOI (7 mm³) were extracted and compared descriptively between the two age and genotype groups. Percentage difference maps were calculated for the changes between baseline and follow-up for the averaged images of $Grn^{-/-}/Tmem106b^{-/-}$ and wild type.

Gene expression profiling and data analysis

Snap-frozen brain hemispheres were mechanically powdered in liquid nitrogen. Following total RNA isolation with the Qiagen RNeasy Mini Kit, 80 ng total RNA per sample was used for gene

expression profiling with the nCounter® Neuropathology panel from NanoString (NanoString Technologies). Expression analysis on the nCounter® Neuroinflammation panel was conducted using 60 ng of total RNA per sample. NanoString reads for all samples were analyzed and normalized using the nSolver software including the R plugin for advanced gene set analysis (NanoString Technologies). The geometric mean of the on-chip housekeeping genes was used for normalization of reads. The mean of each group was used for calculation of the fold changes. For the Neuropathology panel, each group contained an n of three animals. The Neuroinflammation panel was conducted on six wild-type, four $Grn^{-/-}$ and four $Tmem106b^{-/-}$single knockout, and five double knockout $Grn^{-/-}/Tmem106b^{-/-}$ mice. Detailed information on mice used is listed in Table EV1. Volcano plots were generated by plotting the $\log_2$-transformed changes between wild-type and individual groups, against the calculated values of significance with the software GraphPad Prism 8.

Western blotting and antibodies

Mice were PBS perfused, and for biochemically analysis, each brain hemisphere was snap-frozen in liquid nitrogen and mechanically ground to powder. Brain powder was lysed in RIPA buffer (150 mM NaCl, 20 mM Tris–HCl pH 7.4, 1% NP40, 0.05% Triton X-100, 0.5% sodium deoxycholate, 2.5 mM ETDA) using the Precellys lysing kit (Ref.: P00933-LYSK0-A; Bertin Technologies). Supernatants were collected after centrifugation at 17,000 *g*, 4°C, and protein concentration was determined using the bicinchoninic acid assay (Interchim Bioscience). For analysis of TDP-43 and p62, proteins were sequentially isolated as described previously (Gotzl *et al*, 2014). All samples were boiled in Laemmli buffer, and proteins were separated on Tris-glycine gels. Proteins were transferred onto polyvinylidene difluoride membranes or nitrocellulose membranes (both GE Healthcare Life Science). HRP-conjugated antibodies and Pierce™ ECL Plus Western Blotting Substrate (Thermo Fisher Scientific) were used for visualization. The following antibodies were used for Western blotting: TMEM106B (clone 6F2, (Lang *et al*, 2012)), GFAP (DAKO, Z0334), IBA1 (GeneTex, GTX100042), CD68 (Abcam, ab125212), CLEC7A (R&D Systems, AF1756), TREM2 (clone 5F4, (Xiang *et al*, 2016), p62 (MBL, PM045), LC3 (Novusbio, NB100), Ubiquitin (Santa Cruz, clone P4D1), Cathepsin D (Santa Cruz, sc-6486), Cathepsin B (R&D Systems, AF965), Cathepsin L (R&D Systems, AF1515), TDP-43 (Proteintech, 12892-2AP), and Phospho-TDP-43 409/410 (Cosmo Bio Co, CAC-TIP-PTD-M01).

Immunofluorescence and image acquisition

Following deep/lethal anesthesia, animals were PBS perfused. One brain hemisphere was fixed overnight in 4% PFA in PBS (pH = 7.4) and transferred to 30% sucrose in PBS. Brains were processed into 35-µm-thick sagittal sections. Sections were blocked in 4% goat serum and incubated with indicated antibodies of the bellow listed primary antibodies. After several washing steps, sections were incubated with fluorophore conjugated secondary antibodies as indicated (Alexa 488, 594, 647; Thermo Fisher Scientific). After additional washing steps, nuclei were visualized with DAPI. Sections were embedded in Fluoromount™ (Sigma-Aldrich, Merck). Image acquisition was performed on a LEICA DMI-8 with a DFC9000GT camera and the following objectives: (HC PL FL L 20×/0.40 CORR PH1; HC PL APO 40×/0.95 CORR). Confocal Images were acquired on Zeiss LSM 800 Microscope Axio Observer 7 (Objective Plan-Apochromat 63×/1,4 Oil M27). The following antibodies were used for immunofluorescence: GFAP (DAKO, Z0334), IBA1 (GeneTex, GTX100042), CD68 (Abcam, ab125212), CLEC7A (R&D Systems, AF1756), TREM2 (R&D Systems, AF1729), p62 (MBL, PM045), p62 (Progen Biotech GP62C), NeuN (Millipore, MAB377), TDP-43 (Proteintech, 12892-2AP), and Phospho-TDP-43 409/410 (Cosmo Bio Co, CAC-TIP-PTD-M01).

Enzyme activity assay

Fluorescence-based activity assays (Abnova) were used to asses enzyme activity of cathepsin D, cathepsin B, and cathepsin L. Mouse brain powder was homogenized in the recommended lysis buffer and subsequently centrifuged. Cleavage of the quenched fluorescence substrate was continuously measured using the Fluoroskan Ascent FL plate reader (Labsystems).

Statistical analysis

Data were analyzed using GraphPad Prism 8. The rotarod performance is displayed as mean duration on the rotarod from three rounds of testing for each tested animal with standard deviation (SD) of the respective group. Differences between groups were tested by one-way ANOVA with Tukey's *post hoc* test (Figs 1D, 4B, 5B, 6B and C, 7C and 8D). For the analysis of gene expression, the mean of the individual group is compared to the mean of the wild-type controls by two-tailed, unpaired Student's *t*-test (Figs 2A–C and 3A–C). For multiple comparison expression analysis and enzyme activity, all data were normalized to wild type.

Significant differences are indicated as follows in all diagrams: $*P < 0.05$; $**P < 0.01$; $***P < 0.001$; and $****P < 0.0001$.

Data availability

Data sets of raw and processed data produced in this study are available in the following database:

NanoString gene sequence, raw, and processed data:
Gene Expression Omnibus accession number (GSE155065) at https://www.ncbi.nlm.nih.gov/geo/query/acc.cgi?acc = GSE155065
Gene Expression Omnibus accession number (GSE155066) at https://www.ncbi.nlm.nih.gov/geo/query/acc.cgi?acc = GSE155066

Expanded View for this article is available online.

Acknowledgements
This work is supported by the Deutsche Forschungsgemeinschaft (DFG) within the framework of the Munich Cluster for Systems Neurology (EXC 2145 SyNergy; ID 390857198). CH is supported by the Koselleck Project HA1737/16-1 of the DFG (Helmholtz-Gemeinschaft, Zukunftsthema "Immunology and Inflammation" (ZT-0027)). We thank Ramona Rodde for excellent technical assistance. We would like to acknowledge the NanoString EMEA grant program for providing a Neuropathology panel. We would like to thank Dr. M. Nishihara (Department of Veterinary Physiology, The University of Tokyo) for providing the $Grn^{-/-}$ founder mouse strain. Open access funding enabled and organized by ProjektDEAL.

Author contributions

AC, CH, and GW conceived the study and analyzed the results. AC and CH wrote the manuscript with input from all co-authors. GW performed all Western blot assays and immunofluorescence experiments. DE conducted and GW and MS performed behavioral experiments. MD performed the staining of the spinal cord and provided support on immunofluorescence techniques. JG, KW, and MB performed and analyzed TSPO-PET imaging. KF performed RNA isolation and enzyme activity assays. WW consulted and BW generated the *Tmem106b*$^{-/-}$ founder mouse from ES cells.

Conflict of interest

CH collaborates with Denali Therapeutics, participated on one advisory board meeting of Biogen, and received a speaker honorarium from Novartis and Roche. CH is chief advisor of ISAR Bioscience.

References

Ahmed Z, Sheng H, Xu YF, Lin WL, Innes AE, Gass J, Yu X, Wuertzer CA, Hou H, Chiba S *et al* (2010) Accelerated lipofuscinosis and ubiquitination in granulin knockout mice suggest a role for progranulin in successful aging. *Am J Pathol* 177: 311 – 324

Almeida MR, Macario MC, Ramos L, Baldeiras I, Ribeiro MH, Santana I (2016) Portuguese family with the co-occurrence of frontotemporal lobar degeneration and neuronal ceroid lipofuscinosis phenotypes due to progranulin gene mutation. *Neurobiol Aging* 41: 200.e201 – 200

Arrant AE, Nicholson AM, Zhou X, Rademakers R, Roberson ED (2018) Partial Tmem106b reduction does not correct abnormalities due to progranulin haploinsufficiency. *Mol Neurodegener* 13: 32

Baker M, Mackenzie IR, Pickering-Brown SM, Gass J, Rademakers R, Lindholm C, Snowden J, Adamson J, Sadovnick AD, Rollinson S *et al* (2006) Mutations in progranulin cause tau-negative frontotemporal dementia linked to chromosome 17. *Nature* 442: 916 – 919

Bateman A, Cheung ST, Bennett HPJ (2018) A brief overview of progranulin in health and disease. *Methods Mol Biol* 1806: 3 – 15

Beel S, Moisse M, Damme M, De Muynck L, Robberecht W, Van Den Bosch L, Saftig P, Van Damme P (2017) Progranulin functions as a cathepsin D chaperone to stimulate axonal outgrowth *in vivo*. *Hum Mol Genet* 26: 2850 – 2863

Belcastro V, Siciliano V, Gregoretti F, Mithbaokar P, Dharmalingam G, Berlingieri S, Iorio F, Oliva G, Polishchuck R, Brunetti-Pierri N *et al* (2011) Transcriptional gene network inference from a massive dataset elucidates transcriptome organization and gene function. *Nucleic Acids Res* 39: 8677 – 8688

van Blitterswijk M, Mullen B, Nicholson AM, Bieniek KF, Heckman MG, Baker MC, DeJesus-Hernandez M, Finch NA, Brown PH, Murray ME *et al* (2014) TMEM106B protects C9ORF72 expansion carriers against frontotemporal dementia. *Acta Neuropathol* 127: 397 – 406

Brady OA, Zheng Y, Murphy K, Huang M, Hu F (2013) The frontotemporal lobar degeneration risk factor, TMEM106B, regulates lysosomal morphology and function. *Hum Mol Genet* 22: 685 – 695

Brendel M, Probst F, Jaworska A, Overhoff F, Korzhova V, Albert NL, Beck R, Lindner S, Gildehaus FJ, Baumann K *et al* (2016) Glial activation and glucose metabolism in a transgenic amyloid mouse model: a triple-tracer PET study. *J Nucl Med* 57: 954 – 960

Capell A, Liebscher S, Fellerer K, Brouwers N, Willem M, Lammich S, Gijselinck I, Bittner T, Carlson AM, Sasse F *et al* (2011) Rescue of progranulin deficiency associated with frontotemporal lobar degeneration by alkalizing reagents and inhibition of vacuolar ATPase. *J Neurosci* 31: 1885 – 1894

Chang MC, Srinivasan K, Friedman BA, Suto E, Modrusan Z, Lee WP, Kaminker JS, Hansen DV, Sheng M (2017) Progranulin deficiency causes impairment of autophagy and TDP-43 accumulation. *J Exp Med* 214: 2611 – 2628

Chen-Plotkin AS, Unger TL, Gallagher MD, Bill E, Kwong LK, Volpicelli-Daley L, Busch JI, Akle S, Grossman M, Van Deerlin V *et al* (2012) TMEM106B, the risk gene for frontotemporal dementia, is regulated by the microRNA-132/212 cluster and affects progranulin pathways. *J Neurosci* 32: 11213 – 11227

Clayton EL, Milioto C, Muralidharan B, Norona FE, Edgar JR, Soriano A, Jafar-Nejad P, Rigo F, Collinge J, Isaacs AM (2018) Frontotemporal dementia causative CHMP2B impairs neuronal endolysosomal traffic-rescue by TMEM106B knockdown. *Brain* 141: 3428 – 3442

Cruchaga C, Graff C, Chiang HH, Wang J, Hinrichs AL, Spiegel N, Bertelsen S, Mayo K, Norton JB, Morris JC *et al* (2011) Association of TMEM106B gene polymorphism with age at onset in granulin mutation carriers and plasma granulin protein levels. *Arch Neurol* 68: 581 – 586

Cruts M, Gijselinck I, van der Zee J, Engelborghs S, Wils H, Pirici D, Rademakers R, Vandenberghe R, Dermaut B, Martin JJ *et al* (2006) Null mutations in progranulin cause ubiquitin-positive frontotemporal dementia linked to chromosome 17q21. *Nature* 442: 920 – 924

DeJesus-Hernandez M, Mackenzie IR, Boeve BF, Boxer AL, Baker M, Rutherford NJ, Nicholson AM, Finch NA, Flynn H, Adamson J *et al* (2011) Expanded GGGGCC hexanucleotide repeat in noncoding region of C9ORF72 causes chromosome 9p-linked FTD and ALS. *Neuron* 72: 245 – 256

Deussing M, Blume T, Vomacka L, Mahler C, Focke C, Todica A, Unterrainer M, Albert NL, Lindner S, von Ungern-Sternberg B *et al* (2018) Coupling between physiological TSPO expression in brain and myocardium allows stabilization of late-phase cerebral [(18)F]GE180 PET quantification. *NeuroImage* 165: 83 – 91

Feng T, Mai S, Roscoe JM, Sheng RR, Ullah M, Zhang J, Iscol Katz I, Yu H, Xiong W, Hu F (2020a) Loss of TMEM106B and PGRN leads to severe lysosomal abnormalities and neurodegeneration in mice. *EMBO Rep* 21: e50219

Feng T, Sheng RR, Sole-Domenech S, Ullah M, Zhou X, Mendoza CS, Enriquez LCM, Katz II, Paushter DH, Sullivan PM *et al* (2020b) A role of the frontotemporal lobar degeneration risk factor TMEM106B in myelination. *Brain* 143: 2255 – 2271

Finch N, Carrasquillo MM, Baker M, Rutherford NJ, Coppola G, Dejesus-Hernandez M, Crook R, Hunter T, Ghidoni R, Benussi L *et al* (2011) TMEM106B regulates progranulin levels and the penetrance of FTLD in GRN mutation carriers. *Neurology* 76: 467 – 474

Gallagher MD, Suh E, Grossman M, Elman L, McCluskey L, Van Swieten JC, Al-Sarraj S, Neumann M, Gelpi E, Ghetti B *et al* (2014) TMEM106B is a genetic modifier of frontotemporal lobar degeneration with C9orf72 hexanucleotide repeat expansions. *Acta Neuropathol* 127: 407 – 418

Gallagher MD, Posavi M, Huang P, Unger TL, Berlyand Y, Gruenewald AL, Chesi A, Manduchi E, Wells AD, Grant SFA *et al* (2017) A dementia-associated risk variant near TMEM106B alters chromatin architecture and gene expression. *Am J Hum Genet* 101: 643 – 663

Gass J, Cannon A, Mackenzie IR, Boeve B, Baker M, Adamson J, Crook R, Melquist S, Kuntz K, Petersen R *et al* (2006) Mutations in progranulin are a major cause of ubiquitin-positive frontotemporal lobar degeneration. *Hum Mol Genet* 15: 2988 – 3001

Ghoshal N, Dearborn JT, Wozniak DF, Cairns NJ (2012) Core features of frontotemporal dementia recapitulated in progranulin knockout mice. *Neurobiol Dis* 45: 395 – 408

Gotzl JK, Mori K, Damme M, Fellerer K, Tahirovic S, Kleinberger G, Janssens J, van der Zee J, Lang CM, Kremmer E *et al* (2014) Common pathobiochemical hallmarks of progranulin-associated frontotemporal lobar degeneration and neuronal ceroid lipofuscinosis. *Acta Neuropathol* 127: 845 – 860

Gotzl JK, Lang CM, Haass C, Capell A (2016) Impaired protein degradation in FTLD and related disorders. *Ageing Res Rev* 32: 122 – 139

Gotzl JK, Colombo AV, Fellerer K, Reifschneider A, Werner G, Tahirovic S, Haass C, Capell A (2018) Early lysosomal maturation deficits in microglia triggers enhanced lysosomal activity in other brain cells of progranulin knockout mice. *Mol Neurodegener* 13: 48

Gotzl JK, Brendel M, Werner G, Parhizkar S, Sebastian Monasor L, Kleinberger G, Colombo AV, Deussing M, Wagner M, Winkelmann J *et al* (2019) Opposite microglial activation stages upon loss of PGRN or TREM2 result in reduced cerebral glucose metabolism. *EMBO Mol Med* 11: e9711

Guo A, Tapia L, Bamji SX, Cynader MS, Jia W (2010) Progranulin deficiency leads to enhanced cell vulnerability and TDP-43 translocation in primary neuronal cultures. *Brain Res* 1366: 1 – 8

Hara T, Nakamura K, Matsui M, Yamamoto A, Nakahara Y, Suzuki-Migishima R, Yokoyama M, Mishima K, Saito I, Okano H *et al* (2006) Suppression of basal autophagy in neural cells causes neurodegenerative disease in mice. *Nature* 441: 885 – 889

Hardy J, Rogaeva E (2014) Motor neuron disease and frontotemporal dementia: sometimes related, sometimes not. *Exp Neurol* 262(Pt B): 75 – 83

Hasegawa M, Arai T, Nonaka T, Kametani F, Yoshida M, Hashizume Y, Beach TG, Buratti E, Baralle F, Morita M *et al* (2008) Phosphorylated TDP-43 in frontotemporal lobar degeneration and amyotrophic lateral sclerosis. *Ann Neurol* 64: 60 – 70

Holler CJ, Taylor G, Deng Q, Kukar T (2017) Intracellular proteolysis of progranulin generates stable, lysosomal granulins that are haploinsufficient in patients with frontotemporal dementia caused by GRN mutations. *eNeuro* 4: ENEURO.0100-17.2017

Hu F, Padukkavidana T, Vaegter CB, Brady OA, Zheng Y, Mackenzie IR, Feldman HH, Nykjaer A, Strittmatter SM (2010) Sortilin-mediated endocytosis determines levels of the frontotemporal dementia protein, progranulin. *Neuron* 68: 654 – 667

Ikemoto S, Hamano SI, Kikuchi K, Koichihara R, Hirata Y, Matsuura R, Hiraide T, Nakashima M, Inoue K, Kurosawa K *et al* (2020) A recurrent TMEM106B mutation in hypomyelinating leukodystrophy: a rapid diagnostic assay. *Brain Dev* 42: 603 – 606

Kao AW, McKay A, Singh PP, Brunet A, Huang EJ (2017) Progranulin, lysosomal regulation and neurodegenerative disease. *Nat Rev Neurosci* 18: 325 – 333

Kayasuga Y, Chiba S, Suzuki M, Kikusui T, Matsuwaki T, Yamanouchi K, Kotaki H, Horai R, Iwakura Y, Nishihara M (2007) Alteration of behavioural phenotype in mice by targeted disruption of the progranulin gene. *Behav Brain Res* 185: 110 – 118

Klein ZA, Takahashi H, Ma M, Stagi M, Zhou M, Lam TT, Strittmatter SM (2017) Loss of TMEM106B ameliorates lysosomal and frontotemporal dementia-related phenotypes in progranulin-deficient mice. *Neuron* 95: 281 – 296

Kleinberger G, Wils H, Ponsaerts P, Joris G, Timmermans JP, Van Broeckhoven C, Kumar-Singh S (2010) Increased caspase activation and decreased TDP-43 solubility in progranulin knockout cortical cultures. *J Neurochem* 115: 735 – 747

Kleinberger G, Capell A, Haass C, Van Broeckhoven C (2013) Mechanisms of granulin deficiency: lessons from cellular and animal models. *Mol Neurobiol* 47: 337 – 360

Komatsu M, Waguri S, Ueno T, Iwata J, Murata S, Tanida I, Ezaki J, Mizushima N, Ohsumi Y, Uchiyama Y *et al* (2005) Impairment of starvation-induced and constitutive autophagy in Atg7-deficient mice. *J Cell Biol* 169: 425 – 434

Lang CM, Fellerer K, Schwenk BM, Kuhn PH, Kremmer E, Edbauer D, Capell A, Haass C (2012) Membrane orientation and subcellular localization of transmembrane protein 106B (TMEM106B), a major risk factor for frontotemporal lobar degeneration. *J Biol Chem* 287: 19355 – 19365

Le NT, Chang L, Kovlyagina I, Georgiou P, Safren N, Braunstein KE, Kvarta MD, Van Dyke AM, LeGates TA, Philips T *et al* (2016) Motor neuron disease, TDP-43 pathology, and memory deficits in mice expressing ALS-FTD-linked UBQLN2 mutations. *Proc Natl Acad Sci USA* 113: E7580 – E7589

Lee CW, Stankowski JN, Chew J, Cook CN, Lam YW, Almeida S, Carlomagno Y, Lau KF, Prudencio M, Gao FB *et al* (2017) The lysosomal protein cathepsin L is a progranulin protease. *Mol Neurodegener* 12: 55

Li Z, Farias FHG, Dube U, Del-Aguila JL, Mihindukulasuriya KA, Fernandez MV, Ibanez L, Budde JP, Wang F, Lake AM *et al* (2020) The TMEM106B FTLD-protective variant, rs1990621, is also associated with increased neuronal proportion. *Acta Neuropathol* 139: 45 – 61

Liu Y, Pattamatta A, Zu T, Reid T, Bardhi O, Borchelt DR, Yachnis AT, Ranum LP (2016) C9orf72 BAC mouse model with motor deficits and neurodegenerative features of ALS/FTD. *Neuron* 90: 521 – 534

Lui H, Zhang J, Makinson SR, Cahill MK, Kelley KW, Huang HY, Shang Y, Oldham MC, Martens LH, Gao F *et al* (2016) Progranulin deficiency promotes circuit-specific synaptic pruning by microglia via complement activation. *Cell* 165: 921 – 935

Luningschror P, Werner G, Stroobants S, Kakuta S, Dombert B, Sinske D, Wanner R, Lullmann-Rauch R, Wefers B, Wurst W *et al* (2020) The FTLD risk factor TMEM106B regulates the transport of lysosomes at the axon initial segment of motoneurons. *Cell Rep* 30: 3506 – 3519

Murray ME, Cannon A, Graff-Radford NR, Liesinger AM, Rutherford NJ, Ross OA, Duara R, Carrasquillo MM, Rademakers R, Dickson DW (2014) Differential clinicopathologic and genetic features of late-onset amnestic dementias. *Acta Neuropathol* 128: 411 – 421

Nelson PT, Wang WX, Partch AB, Monsell SE, Valladares O, Ellingson SR, Wilfred BR, Naj AC, Wang LS, Kukull WA *et al* (2015) Reassessment of risk genotypes (GRN, TMEM106B, and ABCC9 variants) associated with hippocampal sclerosis of aging pathology. *J Neuropathol Exp Neurol* 74: 75 – 84

Neumann M, Kwong LK, Lee EB, Kremmer E, Flatley A, Xu Y, Forman MS, Troost D, Kretzschmar HA, Trojanowski JQ *et al* (2009) Phosphorylation of S409/410 of TDP-43 is a consistent feature in all sporadic and familial forms of TDP-43 proteinopathies. *Acta Neuropathol* 117: 137 – 149

Nicholson AM, Finch NA, Wojtas A, Baker MC, Perkerson RB 3rd, Castanedes-Casey M, Rousseau L, Benussi L, Binetti G, Ghidoni R *et al* (2013) TMEM106B p. T185S regulates TMEM106B protein levels: implications for frontotemporal dementia. *J Neurochem* 126: 781 – 791

Nicholson AM, Zhou X, Perkerson RB, Parsons TM, Chew J, Brooks M, DeJesus-Hernandez M, Finch NA, Matchett BJ, Kurti A *et al* (2018) Loss of Tmem106b is unable to ameliorate frontotemporal dementia-like phenotypes in an AAV mouse model of C9ORF72-repeat induced toxicity. *Acta Neuropathol Commun* 6: 42

Nixon RA (2013) The role of autophagy in neurodegenerative disease. *Nat Med* 19: 983 – 997

Palmer DN, Barry LA, Tyynela J, Cooper JD (2013) NCL disease mechanisms. *Biochim Biophys Acta* 1832: 1882 – 1893

Petkau TL, Neal SJ, Milnerwood A, Mew A, Hill AM, Orban P, Gregg J, Lu G, Feldman HH, Mackenzie IR *et al* (2012) Synaptic dysfunction in progranulin-deficient mice. *Neurobiol Dis* 45: 711 – 722

Petkau TL, Hill A, Leavitt BR (2016) Core neuropathological abnormalities in progranulin-deficient mice are penetrant on multiple genetic backgrounds. *Neuroscience* 315: 175 – 195

Ren Y, van Blitterswijk M, Allen M, Carrasquillo MM, Reddy JS, Wang X, Beach TG, Dickson DW, Ertekin-Taner N, Asmann YW *et al* (2018) TMEM106B haplotypes have distinct gene expression patterns in aged brain. *Mol Neurodegener* 13: 35

Renton AE, Majounie E, Waite A, Simon-Sanchez J, Rollinson S, Gibbs JR, Schymick JC, Laaksovirta H, van Swieten JC, Myllykangas L *et al* (2011) A hexanucleotide repeat expansion in C9ORF72 is the cause of chromosome 9p21-linked ALS-FTD. *Neuron* 72: 257 – 268

Rhinn H, Abeliovich A (2017) Differential aging analysis in human cerebral cortex identifies variants in TMEM106B and GRN that regulate aging phenotypes. *Cell Syst* 4: 404 – 415

Rutherford NJ, Carrasquillo MM, Li M, Bisceglio G, Menke J, Josephs KA, Parisi JE, Petersen RC, Graff-Radford NR, Younkin SG *et al* (2012) TMEM106B risk variant is implicated in the pathologic presentation of Alzheimer disease. *Neurology* 79: 717 – 718

Sardiello M, Palmieri M, di Ronza A, Medina DL, Valenza M, Gennarino VA, Di Malta C, Donaudy F, Embrione V, Polishchuk RS *et al* (2009) A gene network regulating lysosomal biogenesis and function. *Science* 325: 473 – 477

Schwenk BM, Lang CM, Hogl S, Tahirovic S, Orozco D, Rentzsch K, Lichtenthaler SF, Hoogenraad CC, Capell A, Haass C *et al* (2014) The FTLD risk factor TMEM106B and MAP6 control dendritic trafficking of lysosomes. *EMBO J* 33: 450 – 467

Settembre C, Ballabio A (2011) TFEB regulates autophagy: an integrated coordination of cellular degradation and recycling processes. *Autophagy* 7: 1379 – 1381

Settembre C, Di Malta C, Polito VA, Garcia Arencibia M, Vetrini F, Erdin S, Erdin SU, Huynh T, Medina D, Colella P *et al* (2011) TFEB links autophagy to lysosomal biogenesis. *Science* 332: 1429 – 1433

Smith KR, Damiano J, Franceschetti S, Carpenter S, Canafoglia L, Morbin M, Rossi G, Pareyson D, Mole SE, Staropoli JF *et al* (2012) Strikingly different clinicopathological phenotypes determined by progranulin-mutation dosage. *Am J Hum Genet* 90: 1102 – 1107

Snowden JS, Pickering-Brown SM, Mackenzie IR, Richardson AM, Varma A, Neary D, Mann DM (2006) Progranulin gene mutations associated with frontotemporal dementia and progressive non-fluent aphasia. *Brain* 129: 3091 – 3102

Stagi M, Klein ZA, Gould TJ, Bewersdorf J, Strittmatter SM (2014) Lysosome size, motility and stress response regulated by fronto-temporal dementia modifier TMEM106B. *Mol Cell Neurosci* 61: 226 – 240

Tanaka Y, Matsuwaki T, Yamanouchi K, Nishihara M (2013) Increased lysosomal biogenesis in activated microglia and exacerbated neuronal damage after traumatic brain injury in progranulin-deficient mice. *Neuroscience* 250: 8 – 19

Tanaka Y, Chambers JK, Matsuwaki T, Yamanouchi K, Nishihara M (2014) Possible involvement of lysosomal dysfunction in pathological changes of the brain in aged progranulin-deficient mice. *Acta Neuropathol Commun* 2: 78

Tanaka Y, Suzuki G, Matsuwaki T, Hosokawa M, Serrano G, Beach TG, Yamanouchi K, Hasegawa M, Nishihara M (2017) Progranulin regulates lysosomal function and biogenesis through acidification of lysosomes. *Hum Mol Genet* 26: 969 – 988

Van Deerlin VM, Sleiman PM, Martinez-Lage M, Chen-Plotkin A, Wang LS, Graff-Radford NR, Dickson DW, Rademakers R, Boeve BF, Grossman M *et al* (2010) Common variants at 7p21 are associated with frontotemporal lobar degeneration with TDP-43 inclusions. *Nat Genet* 42: 234 – 239

Ward ME, Chen R, Huang HY, Ludwig C, Telpoukhovskaia M, Taubes A, Boudin H, Minami SS, Reichert M, Albrecht P *et al* (2017) Individuals with progranulin haploinsufficiency exhibit features of neuronal ceroid lipofuscinosis. *Sci Transl Med* 9: eaah5642

Wils H, Kleinberger G, Janssens J, Pereson S, Joris G, Cuijt I, Smits V, Ceuterick-de Groote C, Van Broeckhoven C, Kumar-Singh S (2010) TDP-43 transgenic mice develop spastic paralysis and neuronal inclusions characteristic of ALS and frontotemporal lobar degeneration. *Proc Natl Acad Sci USA* 107: 3858 – 3863

Wils H, Kleinberger G, Pereson S, Janssens J, Capell A, Van Dam D, Cuijt I, Joris G, De Deyn PP, Haass C *et al* (2012) Cellular ageing, increased mortality and FTLD-TDP-associated neuropathology in progranulin knockout mice. *J Pathol* 228: 67 – 76

Xiang X, Werner G, Bohrmann B, Liesz A, Mazaheri F, Capell A, Feederle R, Knuesel I, Kleinberger G, Haass C (2016) TREM2 deficiency reduces the efficacy of immunotherapeutic amyloid clearance. *EMBO Mol Med* 8: 992 – 1004

Yin F, Banerjee R, Thomas B, Zhou P, Qian L, Jia T, Ma X, Ma Y, Iadecola C, Beal MF *et al* (2010a) Exaggerated inflammation, impaired host defense, and neuropathology in progranulin-deficient mice. *J Exp Med* 207: 117 – 128

Yin F, Dumont M, Banerjee R, Ma Y, Li H, Lin MT, Beal MF, Nathan C, Thomas B, Ding A (2010b) Behavioral deficits and progressive neuropathology in progranulin-deficient mice: a mouse model of frontotemporal dementia. *FASEB J* 24: 4639 – 4647

Yu L, De Jager PL, Yang J, Trojanowski JQ, Bennett DA, Schneider JA (2015) The TMEM106B locus and TDP-43 pathology in older persons without FTLD. *Neurology* 84: 927 – 934

van der Zee J, Van Langenhove T, Kleinberger G, Sleegers K, Engelborghs S, Vandenberghe R, Santens P, Van den Broeck M, Joris G, Brys J *et al* (2011) TMEM106B is associated with frontotemporal lobar degeneration in a clinically diagnosed patient cohort. *Brain* 134: 808 – 815

Zhou X, Sun L, Bastos de Oliveira F, Qi X, Brown WJ, Smolka MB, Sun Y, Hu F (2015) Prosaposin facilitates sortilin-independent lysosomal trafficking of progranulin. *J Cell Biol* 210: 991 – 1002

Zhou X, Paushter DH, Feng T, Pardon CM, Mendoza CS, Hu F (2017a) Regulation of cathepsin D activity by the FTLD protein progranulin. *Acta Neuropathol* 134: 151 – 153

Zhou X, Paushter DH, Feng T, Sun L, Reinheckel T, Hu F (2017b) Lysosomal processing of progranulin. *Mol Neurodegener* 12: 62

Zhou X, Brooks M, Jiang P, Koga S, Zuberi AR, Baker MC, Parsons TM, Castanedes-Casey M, Phillips V, Librero AL *et al* (2020a) Loss of Tmem106b exacerbates FTLD pathologies and causes motor deficits in progranulin deficient mice. *EMBO Rep* 21: e50197

Zhou X, Nicholson AM, Ren Y, Brooks M, Jiang P, Zuberi A, Phuoc HN, Perkerson RB, Matchett B, Parsons TM *et al* (2020b) Loss of TMEM106B leads to myelination deficits: implications for frontotemporal dementia treatment strategies. *Brain* 143: 1905 – 1919